SYNTHESIS OF HEAVY ELEMENTS

- NOT BY FUSION REACTIONS but POSSIBLE at SITES WHERE FUSION REACTIONS ARE OCCURING
- KEY IS NEUTRON CAPTURE REACTIONS
  - POSSIBLY ADJUNCT OF FUSION REACTIONS

THREE TYPES OF SYNTHESIS

- s- PROCESS(ES)
- r - PROCESS(ES)
- p - NUCLEI

→

NUCLIDES WHICH ARE:

s- only

r- only

s+r

p - only

ELEMENTS ARE A MIX but a few are almost 'pure'

e.g.

Ba ≃ s-only

Eu ≃ r-only

SUGGESTED SITES

S-PROCESS →

MASSIVE STARS → WEAK S-PROCESS

- He-CORE BURNING
- C-SHELL BURNING

LOW & IM AGB STARS

→ MAIN + STRONG S-PROCESS

- He-SHELL PULSES

r-PROCESS →

SN II

MERGING NEUTRON STARS

} WHICH OR BOTH ?

P-PROCESS →

? - FEW NUCLIDES

- NO ELEMENT DOMINATED BY P-PROCESS

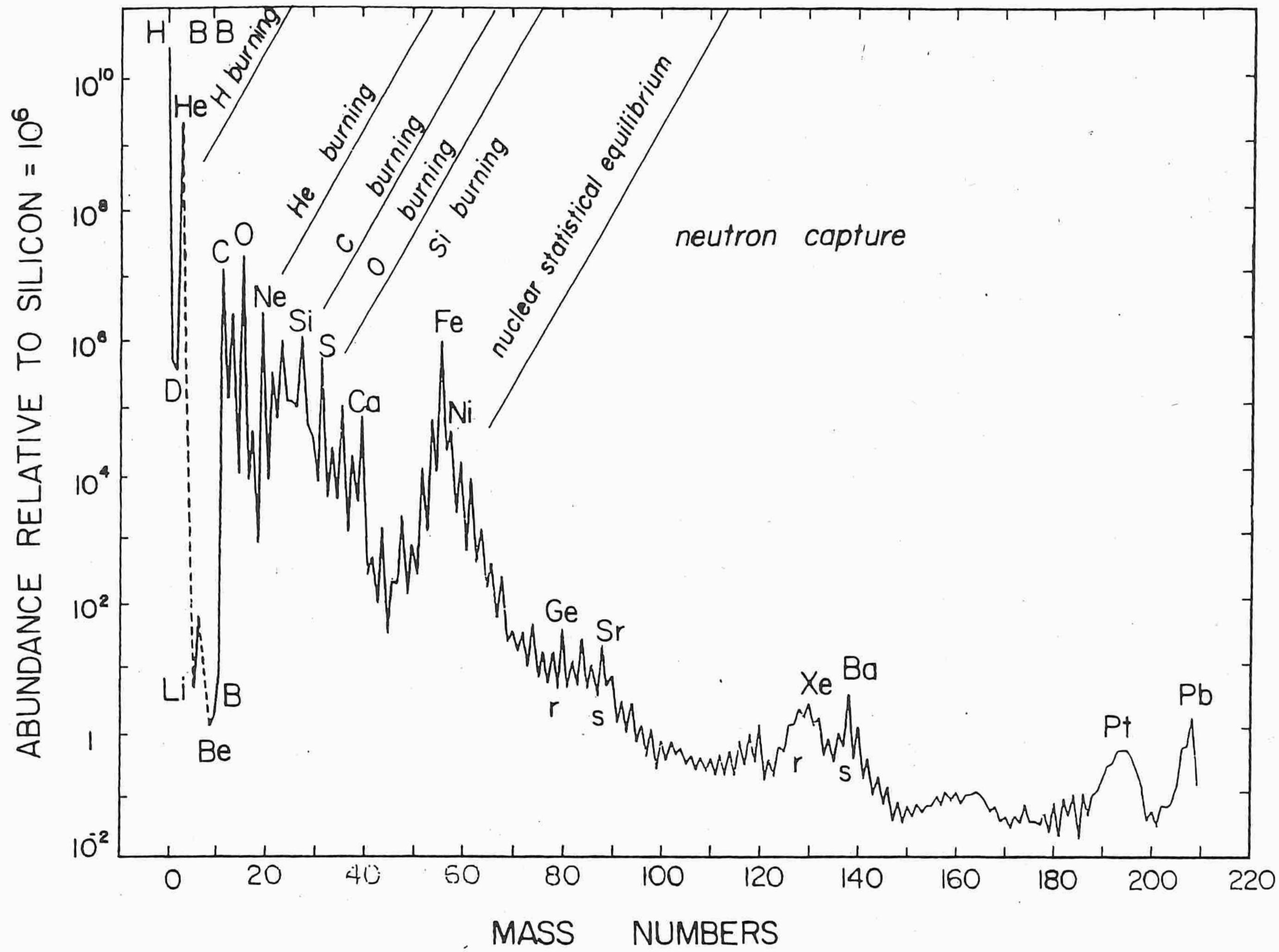

Fig. 1.4. The 'local Galactic' abundance distribution of nuclear species, normalized to 10^6 ^{28}Si atoms, adapted from Cameron (1982).

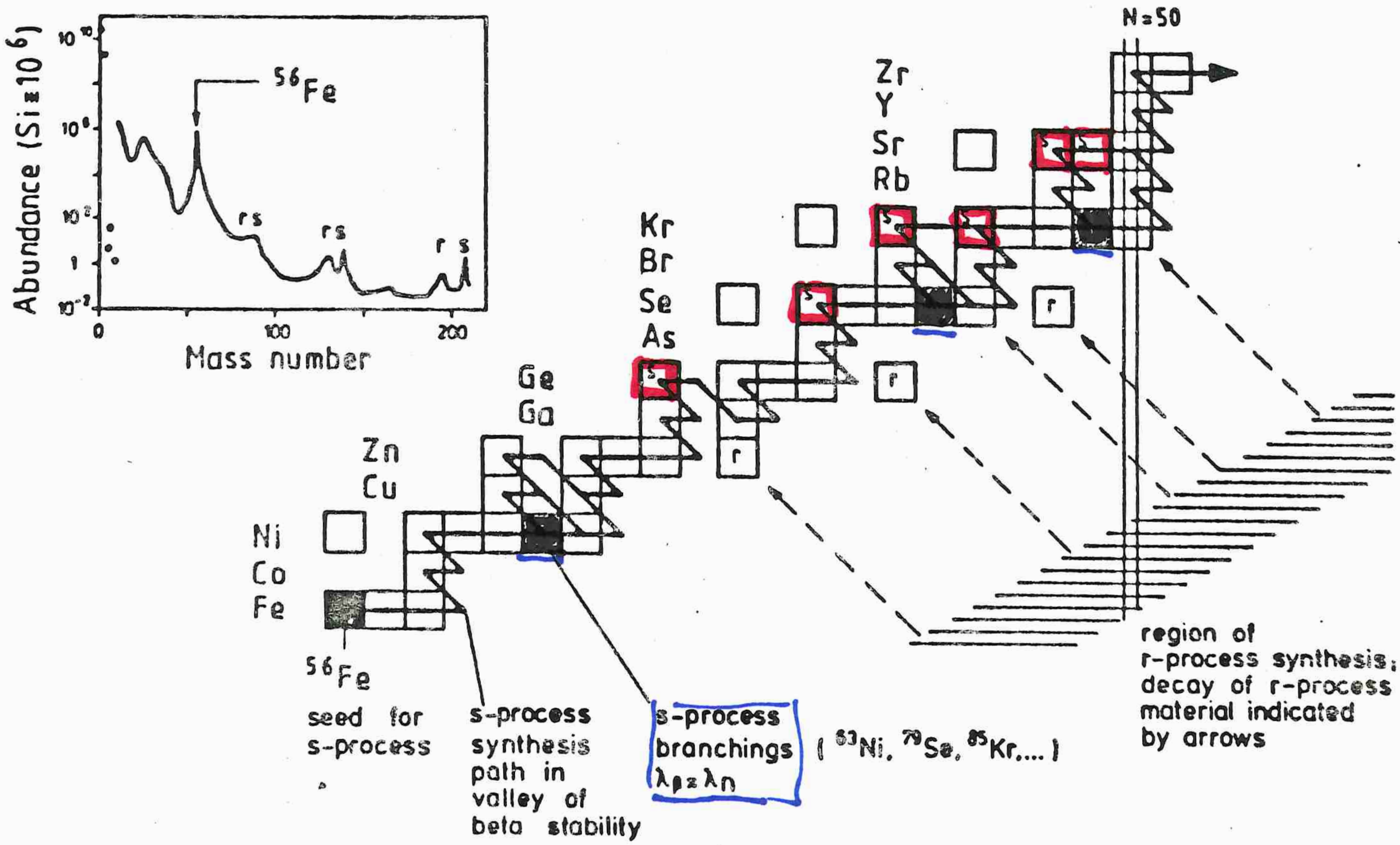

Figure 1. Section of the chart of nuclides for a discussion of the main features of neutron capture nucleosynthesis (see text).

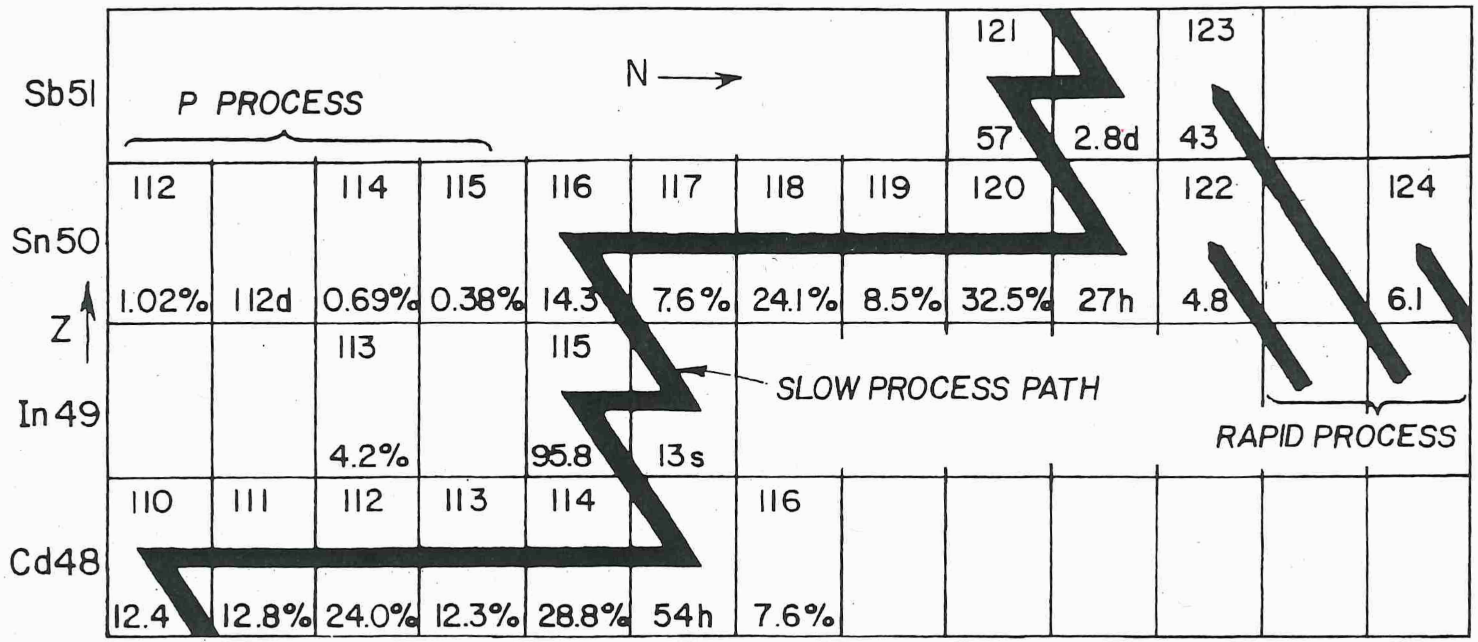

Fig. 1.5. Paths of the r-, s- and p-processes in the neighbourhood of the tin isotopes. Numbers in the boxes give mass numbers and percentage abundance of the isotope for stable species, and β-decay lifetimes for unstable ones. ^{116}Sn is an s-only isotope, shielded from the r-process by ^{116}Cd. After Clayton *et al.* (1961). Copyright by Academic Press, Inc. Courtesy Don Clayton.

STELLAR OBSERVATIONS

- S-PROCESS
  - STARS WITH NATAL COMPOSITION
    - Ba et al. as function of [Fe/H], location, ...
  - STARS self-enriched
    - cool AGB stars (Tc!)
    - post AGB stars
    - PN
  - STARS polluted by a companion
    - Ba II, CH giants

- r - PROCESS
  - STARS WITH NATAL COMPOSITION
    - Eu et al. as function of [Fe/H], location

(separate from s-process)

  - STARS polluted heavily
    - companion, local cloud enriched
    - very r-process enriched *s
    - very r-process rich stars in dwarf galaxy

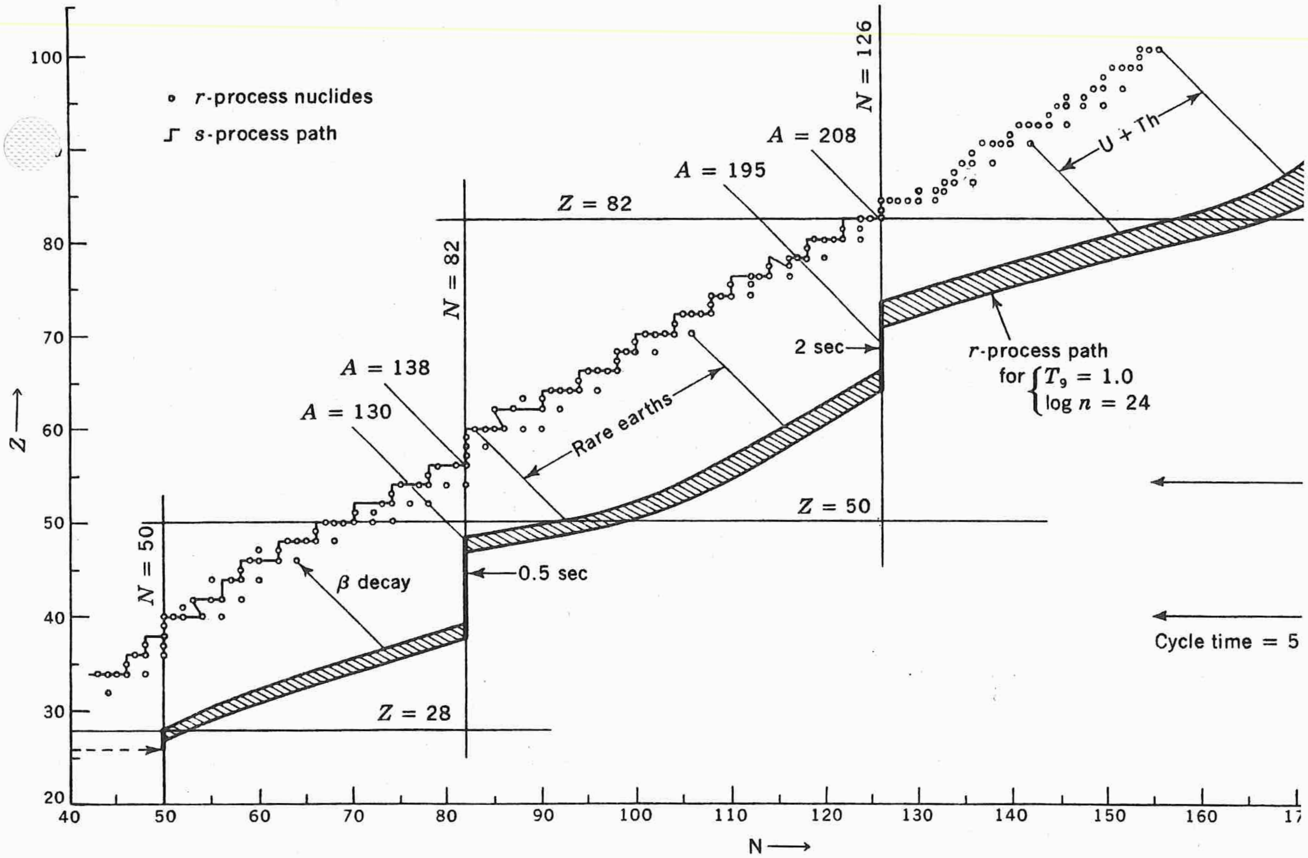

Fig. 7-30 Neutron-capture paths for the s process and the r process. The s process follows a path in the NZ plane along the li
·e neutron-rich progenitors to the stable r-process nuclei, which are here shown as small circles, are formed in a band in the r
.e NZ plane, such as the shaded area shown here. This r-process path was calculated for the case $T_9 = 1.0$ and $\log n_n = 24$. .
ing event the nuclei in this band beta-decay to the stable r-process nuclei. The abundance peaks at $A = 80$, 130, and 195 are
dance peaks in the neutron-rich progenitors having $N = 50$, 82, and 126. Neutron capture flows upward from the lower left-ha
shaded band until neutron-induced fission occurs near $A = 270$. [*P. A. Seeger, W. A. Fowler, and D. D. Clayton, Astrophy*
(1965). *By permission of The University of Chicago Press. Copyright* 1965 *by The University of Chicago.*]

OLD SCHEMATIC to show why r-PROCESS PEAK IS TO LOWER MASS NUMBER THAN s-PROCESS PEAK

S-PROCESS - BASICS

- $\sigma(n,\gamma)$
  - NO COULOMB BARRIER
  - $\sigma \propto$ TIME TO CROSS NUCLEUS

    $\sigma \propto t \propto \frac{1}{v}$ $\sigma v \sim$ const.
  - DEPENDS ON STRUCTURE OF NUCLEUS

    σ SMALL for N = magic no.

    Z = odd = even differences
  - MANY σ's WELL MEASURED BUT ONLY NUCLEAR GROUND STATES

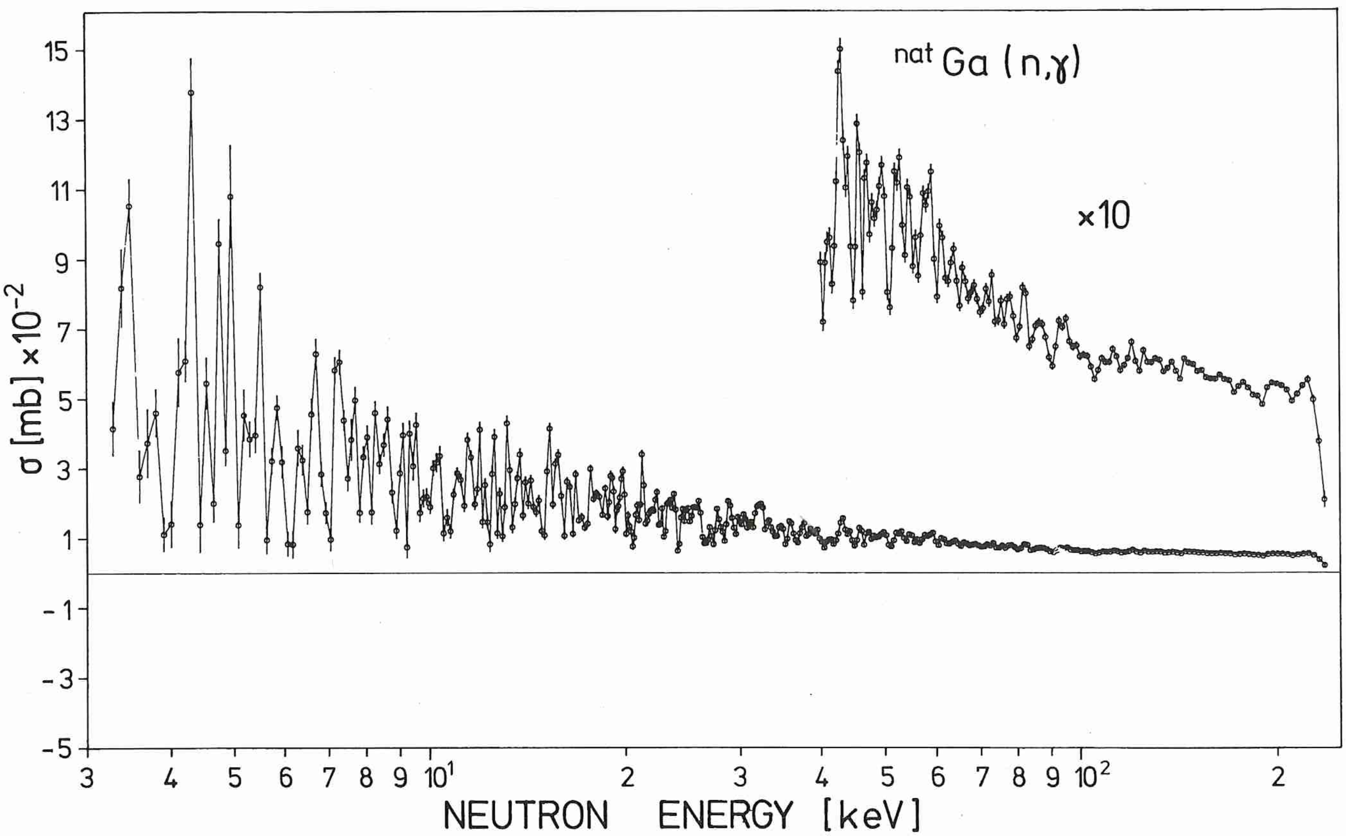

Fig. 4. Capture cross section of ^{nat}Ga as a function of neutron energy

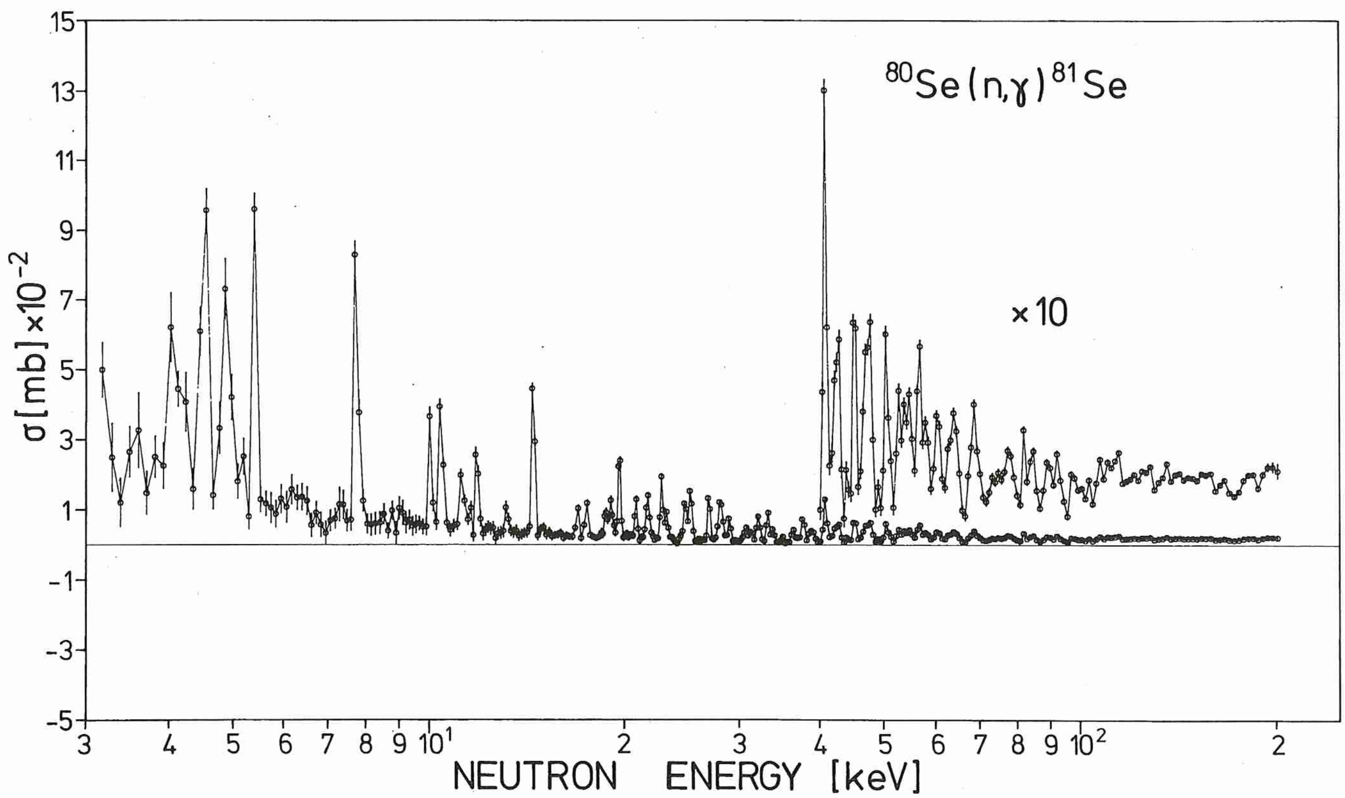

Fig. 5. Capture cross section of ^{80}Se as a function of neutron energy

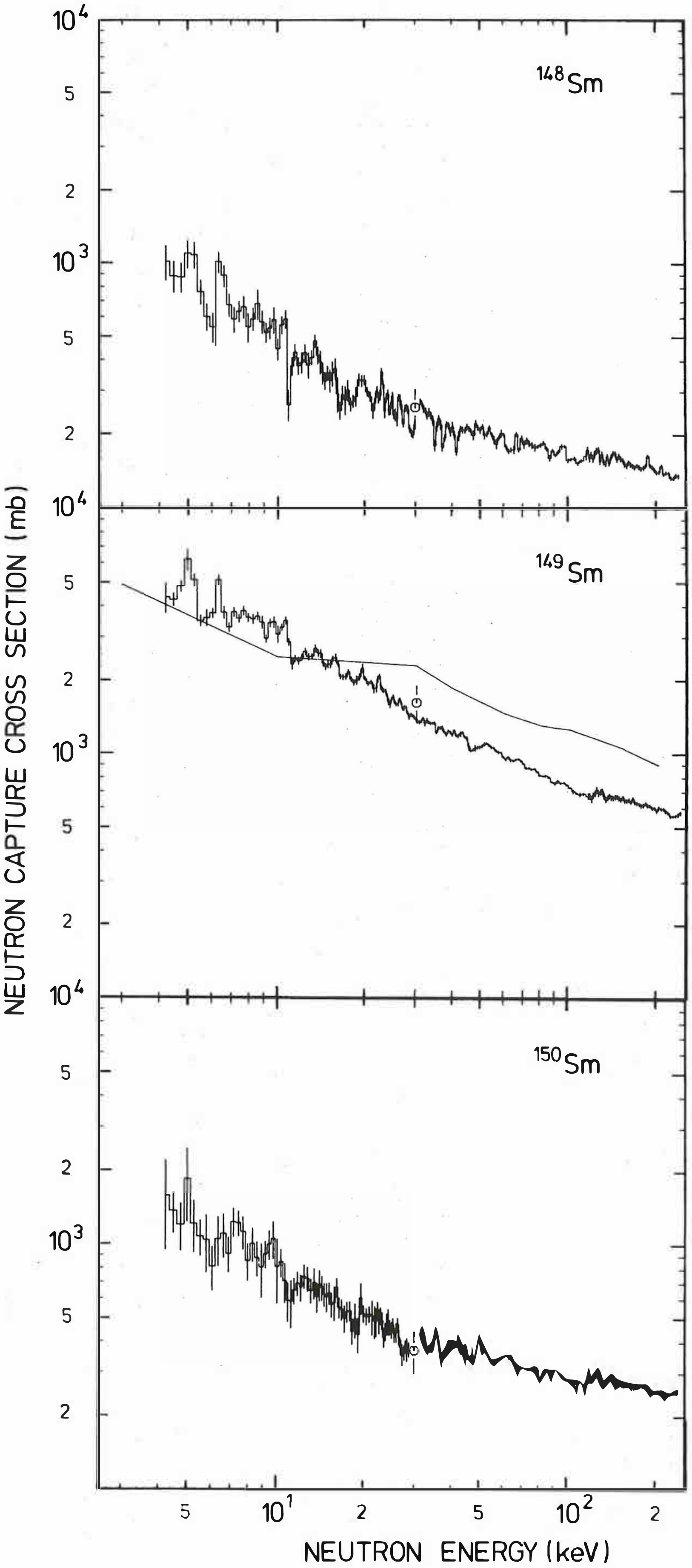

FIG. 3.—Neutron capture cross sections of $^{148,149,150}Sm$ obtained in this work. The 30 keV values of Macklin, Gibbons, and Inada (1963) are shown for comparison (*open circles*). For ^{149}Sm the ENDF/B-V evaluation is also included (*solid line*).

approximately the v^{-1} dependence. The following table constructed from their Table 8 shows that $<\sigma v>$ is nearly a constant:

kT (keV)	^{148}Sm $<\sigma>$ (mb)	$<\sigma v>/<\sigma v>_{10keV}$	
10	522 ± 26	1.0	
20	339 ± 16	1.09	N.B. 1.0 to within experimental error
30	277 ± 13	1.09	
50	225 ± 10	1.04	
100	174 ± 8	1.05	

The agreement is not so spectacular for ^{149}Sm and ^{150}Sm! Note: the measured cross-sections must be extrapolated in order to compute $<\sigma v>$'s.

Our second example (Figures 4, 5) is taken from Walter *et al.* (1986, *Astr. Ap.*, **167**, 186). These σ's show much more structure (resonances) imposed upon a roughly v^{-1} decline. However, the Maxwellian velocity distribution 'smooths' out the resonances and $<\sigma v>$ is again nearly independent of temperature. The following table is adapted from Walter *et. al.*'s Table 8:

kT (keV)	^{80}Se $<\sigma>$ (mb)	$<\sigma v>/<\sigma v>_{20keV}$	
20	57 ± 4	1.0	N.B. 1.0 to within experimental error
30	44 ± 3	0.95	
40	38 ± 3	0.94	
50	34 ± 3	0.94	

For an introduction to current measurement techniques, see Käppeler's chapter in "Nucleosynthesis: Challenges and New Developments".

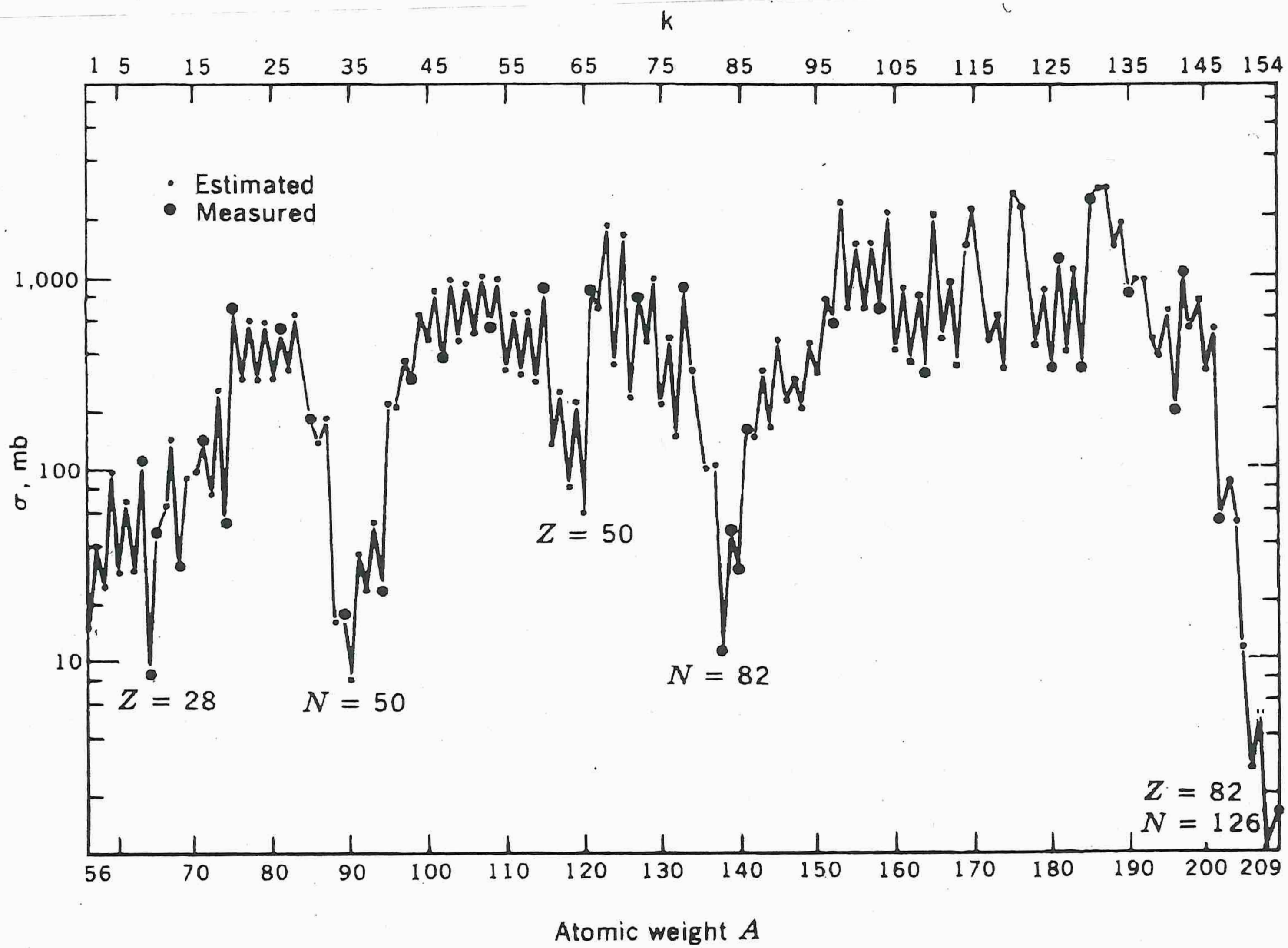

Fig. 6.2. Neutron-capture cross-sections at energies near 25 keV. Very large dips occur at the magic numbers. After Clayton (1984). Copyright by the University of Chicago. Courtesy Don Clayton.

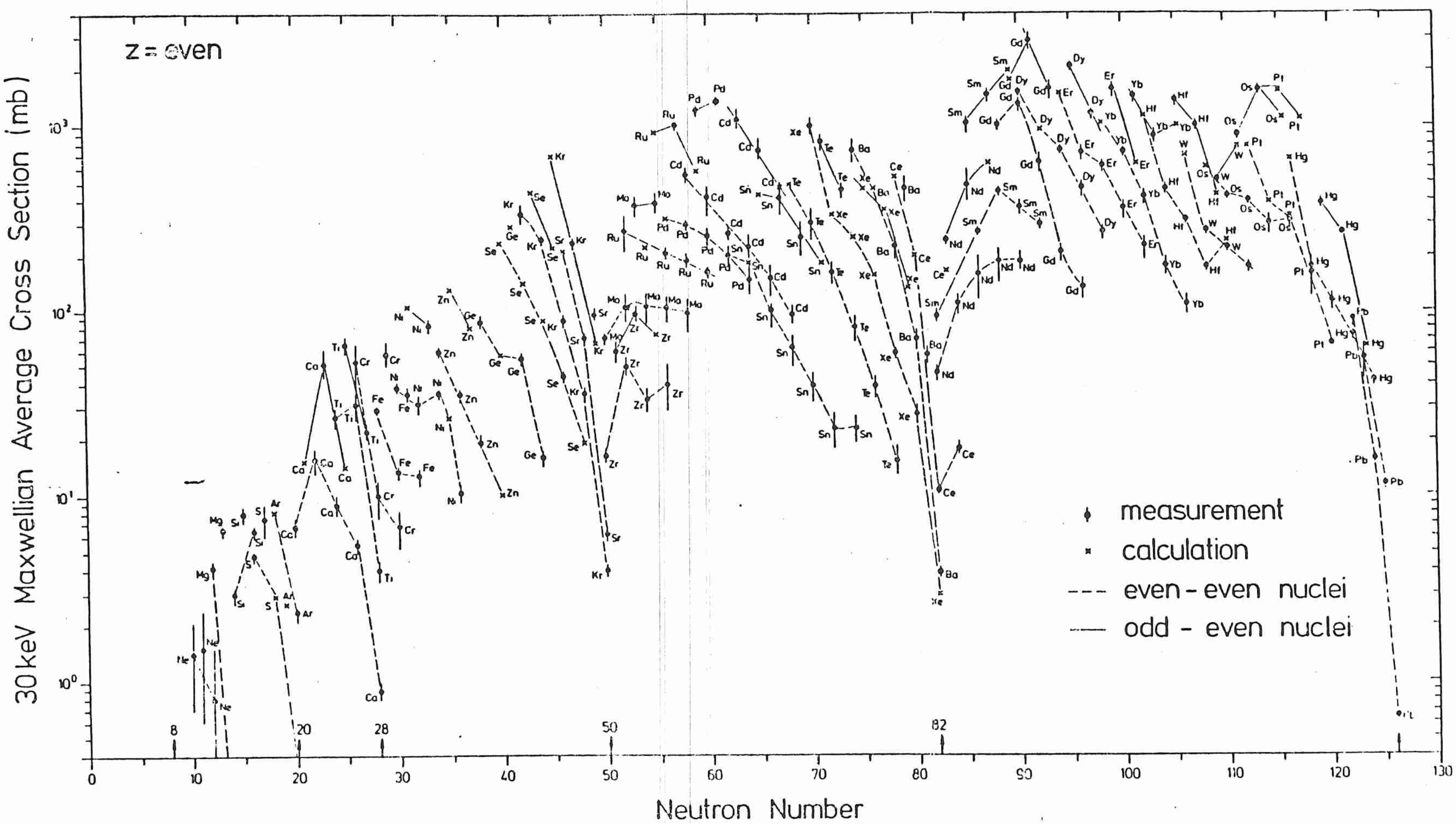

Fig. 1 Maxwellian average neutron capture cross sections for kT = 30 keV of isotopes with even Z.

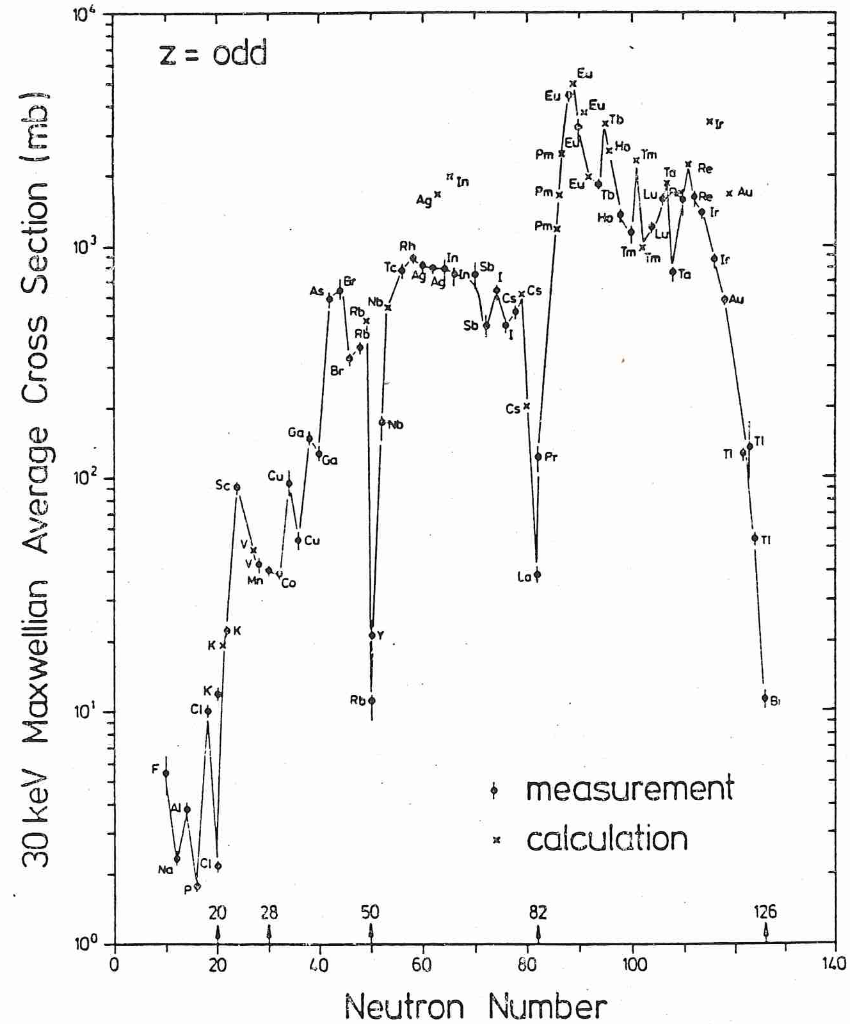

Fig. 2 Maxwellian average neutron capture cross sections for kT = 30 keV of isotopes with odd Z.

S-PROCESS · BASICS

$\sigma \propto \frac{1}{v}$ $\therefore \langle \sigma v \rangle \sim$ constant

See examples of ^{148}Sm and ^{80}Se

— σ COMPILATIONS

See KÄPPELER et al. RMP 83 157 2011

http://www.kadonis.org

σ EXPT + THEORY → σ RECOMM.

MACS at various kT

STELLAR ENHANCEMENT FACTOR

RATE CONSTANTS

updated ?

Karlsruhe Astrophysical Database of Nucleosynthesis in Stars

▼ Available isotopes for Barium (Z=56)

^{130}Ba ^{132}Ba ^{134}Ba ^{135}Ba ^{136}Ba ^{137}Ba ^{138}Ba

Go to isotope [ ] Go!

▼ Recommended MACS30 (Maxwellian Averaged Cross Section @ 30keV)

$$^{138}Ba\ (n,\gamma)^{139}Ba$$

Total MACS at 30keV: 4.00 ± 0.20 mb

Cross sections do not include stellar enhancement factors!

▼ History

Version	Total MACS [mb]	Partial to gs [mb]	Partial to isomer [mb]
0.0	4.00 ± 0.20	-	-

(Version 0.0 corresponds to Bao et al.)

▼ Comment

Last review: 2000

▼ List of all available values

original	renorm.	year	type	Comment	Ref
4.07 ± 0.20		1997	c	Linac, TOF, ^{6}Li, Au+Ag:Sat.	BCM97
4.22 ± 0.25	3.93	1980	c	VdG, Act., 1/v(kT), Au:B-IV	BeK80
3.8 ± 0.8		1979	c,2	Linac, TOF, ^{6}Li, Au:Sat., k=0.9833	MAM79
5 ± 2		1977	c	Linac, TOF, ^{6}Li+^{235}U, Au:Sat.	MAB75,MAB77a
12.6 ± 1.6 23keV	9.5	1973	c	Sb-Be, Act., 1/v(E), ^{127}I:836mb(23keV)	SSR73
8 ± 2		1971	e		AGM71
3.75		2006	e		endfb7
4.30		2004	e		jeff31
4.30		2002	e		jendl33
6.3		2000	t		RaT99
4.8		1981	t		Har81
6.7		1976	t		HWF76

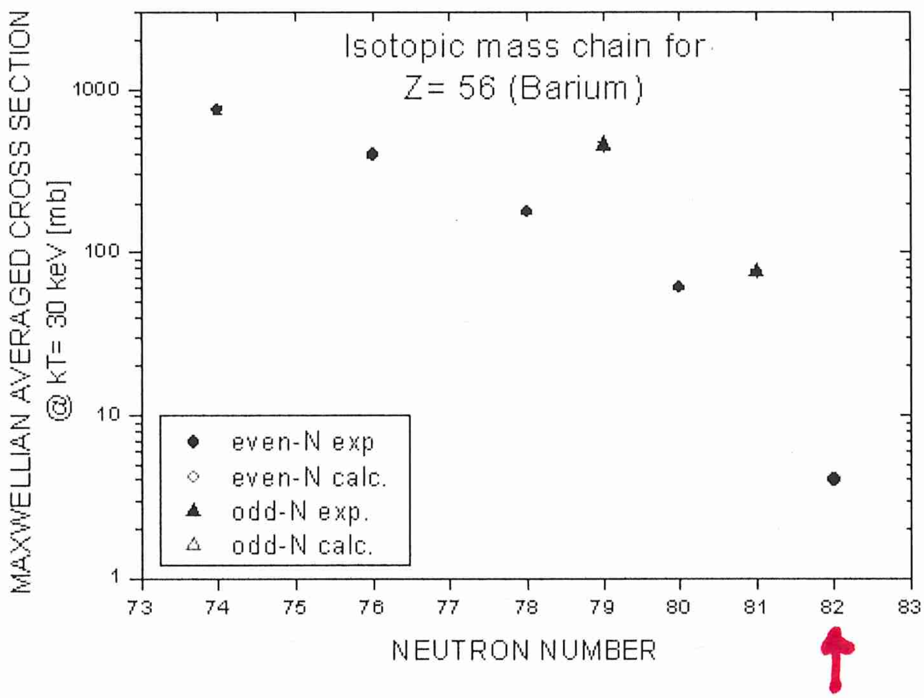

▼ Chart of nuclei

^{138}Ce 0.251 179 mb	^{139}Ce 137.62 d 214 mb, β+	^{140}Ce 88.45 11 mb	^{141}Ce 32.51 d 76 mb, β-	^{142}Ce 11.114 28 mb
^{137}La 59.99 ka β+	^{138}La 102.01x10^{9} y 419 mb, β+	^{139}La 99.91 31.6 mb	^{140}La 1.68 d β-	^{141}La 3.92 h β-
^{136}Ba **7.854** **61.2 mb**	^{137}Ba 11.232 76.3 mb	^{138}Ba 71.698 4 mb	^{139}Ba 1.38 h β-	^{140}Ba 12.75 d β-
^{135}Cs 2.30 Ma 198 mb, β-	^{136}Cs 13.04 d β-	^{137}Cs 30.03 a β-	^{138}Cs 33.41 m β-	^{139}Cs 9.27 m β-
^{134}Xe 10.436 20.2 mb	^{135}Xe 9.14 h β-	**^{136}Xe** **8.857** **0.91 mb**	^{137}Xe 3.82 m β-	^{138}Xe 14.08 m β-

Style: (Size: S, M, L, XL, Alberto; No-Macs: nox) Refresh

D. Status and Prospects

from Käppeler et al. (2011)

1. Compilations of stellar (n,γ) cross sections and further requirements

Stellar neutron capture cross sections have first been compiled in 1971 by Allen *et al.* (1971), who presented a set of recommended (n,γ) cross sections averaged over a Maxwell-Boltzmann distribution for a thermal energy of $kT =$ 30 keV. This first collection of Maxwellian averaged cross sections (MACS) comprised already 130 experimental cross sections with typical uncertainties between 10 and 25%. These data were complemented by 109 semi-empirical values estimated from the cross section trends with neutron number of neighboring nuclei to provide a full set of nuclear data for quantitative studies of the *s*-process.

The next compilation of experimental and theoretical stellar neutron cross sections for *s*-process studies, which was published 16 years later by Bao and Käppeler (1987), included cross sections for (n,γ) reactions between ^{12}C and ^{209}Bi, some (n,p) and (n,α) reactions (from ^{33}Se to ^{59}Ni), and also (n,γ) and (n,f) reactions for long-lived actinides. Also in this version MACSs were given at a single thermal energy of $kT = 30$ keV, sufficient for studies with the canonical *s*-process formulated by Seeger *et al.* (1965) for a constant temperature and neutron density scenario. A major achievement, however, was the significant improvement of the accuracy, which was reaching the 1 - 2% level for a number of important *s*-process isotopes.

Meanwhile, the canonical or "classical" approach had been challenged by refined stellar models, which indicated different sites for the *s*-process, from He shell burning in thermally pulsing low mass AGB stars (Gallino *et al.*, 1988; Hollowell and Iben, 1988) to shell C burning in massive stars (Raiteri *et al.*, 1991a,b), where (α,n) reactions on ^{13}C and ^{22}Ne were identified as the dominant neutron sources, respectively. The fact that the temperatures at the various sites require MACS data for thermal energies between 8 and 90 keV was taken into account in the compilation of Beer *et al.* (1992a), which listed values in the range $5 \leq kT \leq 100$ keV.

The following compilation of Bao *et al.* (2000) was extended to cover a network of 364 (n,γ) reactions, including also relevant partial cross sections. This work presents detailed information on previous MACS results, which were eventually condensed into recommended values. Again, data are given for thermal energies from 5 to 100 keV. For isotopes without experimental cross section information, recommended values were derived from calculations with the Hauser-Feshbach statistical model code NON-SMOKER (Rauscher and Thielemann, 2000), which were empirically corrected for known systematic deficiencies in the nuclear input of the calculation. For the first time, stellar enhancement factors (SEF), which take the effect of thermally excited nuclear states into account, were included as well.

For easy access, the compilation of Bao *et al.* (2000) was published in electronic form via the KADoNiS project (http://www.kadonis.org) (Dillmann *et al.*, 2005). The current version KADoNiS v0.3 (Dillmann *et al.*, 2009) is already the third update and includes – compared to the Bao *et al.* compilation (Bao *et al.*, 2000) – recommended values for 38 improved and 14 new cross sections. In total, data sets are available for 356 isotopes, including 77 radioactive nuclei on or close to the *s*-process path. For 13 of these radioactive nuclei, experimental data is available, i.e. for ^{14}C, ^{60}Fe, ^{93}Zr, ^{99}Tc, ^{107}Pd, ^{129}I, ^{135}Cs, ^{147}Pm, ^{151}Sm, ^{155}Eu, ^{163}Ho, ^{182}Hf, and ^{185}W. The remaining 64 radioactive nuclei are not (yet) measured in the stellar energy range and are represented only by empirically corrected Hauser-Feshbach rates with typical uncertainties of 25 to 30%. Almost all of the (n,γ) cross sections of the 277 stable isotopes have been measured. The few exceptions are ^{17}O, ^{36,38}Ar, ^{40}K, ^{50}V, ^{70}Zn, ^{72,73}Ge, ^{77,82}Se, ^{98,99}Ru, ^{131}Xe, ^{138}La, ^{158}Dy, and ^{195}Pt, which lie mostly outside the *s*-process path in the proton-rich *p*-process domain. These cross sections are difficult to determine because they are often not accessible by activation measurements or not available in sufficient amounts and/or enrichment for time-of-flight measurements.

The actual status of the (n,γ) cross sections for *s*-process nucleosynthesis calculations is summarized in Fig. 6, which shows the respective uncertainties as a function of mass number. Though the necessary accuracy of 1 to 5% has been locally achieved, further improvements are clearly required, predominantly in the mass region below $A =$ 120 and above $A = 180$.

Further efforts in this field are the more important as Fig. 6 reflects only the situation for a thermal energy of 30 keV. In most cases, however, extrapolation to lower and higher temperatures implies still larger uncertainties.

The lack of accurate data is particularly crucial for the weak *s*-process in massive stars, which is responsible for most of the *s* abundances between Cu and Sr. Since the neutron exposure of the the weak *s* process is not sufficient for achieving flow equilibrium, cross section uncertainties may affect the abundances of a sequence of heavier isotopes (see Sec. III.B).

The present version of KADoNiS consists of two parts: the *s*-process library and a collection of available experimental *p*-process reactions. The *s*-process library will be complemented in the near future by some (n,p) and (n,α) cross sections measured at $kT = 30$ keV, as it was already included in (Bao and Käppeler, 1987). The *p*-process database will be a collection of all available charged-particle reactions measured within or close to the Gamow window of the *p* process (T_9= 2-3 GK).

In a further extension of KADoNiS it is planned to include more radioactive isotopes, which are relevant for *s*-process nucleosynthesis at higher neutron densities (up to 10^{11} cm^{-3}) (Cristallo *et al.*, 2006). Since these isotopes are more than one atomic mass unit away from the "regular" *s*-process path on the neutron-rich side of stability, their stellar (n,γ) values have to be extrapolated from known cross sections by means of the statistical Hauser-Feshbach model. The present list covers 73 new isotopes and is available on the KADoNiS homepage.

TIME SCALE ?

$^{56}Fe \rightarrow {}^{209}Bi$ 153 neutrons

- TIME LARGELY CONTROLLED BY σ AT N = MAGIC, $\sigma \sim 10\,mb$
- TAKE $N(n) \sim 10^{8}\,cm^{-3}$
  $T \sim 2\times10^{8}K$ or $E \sim 30\,keV$
  $\rightarrow \tau_n \sim 100$ yrs for $\sigma = 10\,mb$
- $\tau_s \sim 150\,\tau_n = 2\times10^{4}$ yrs
  $\cong$ AGB TP phase

BRANCHES - half-life against n-capture

$$\tau_n = \frac{\ln 2}{N(n)\langle\sigma v\rangle}$$

$\sigma \sim 1000$ mb
$= 10^{-24}$ cm^2

away from N=magic

$v \sim 2 \times 10^8$ cm/s

τ_n [yr]	$N(n)$ cm^{-3}
1	7.3, 7
10^2	7.3, 5
10^4	7.3, 3

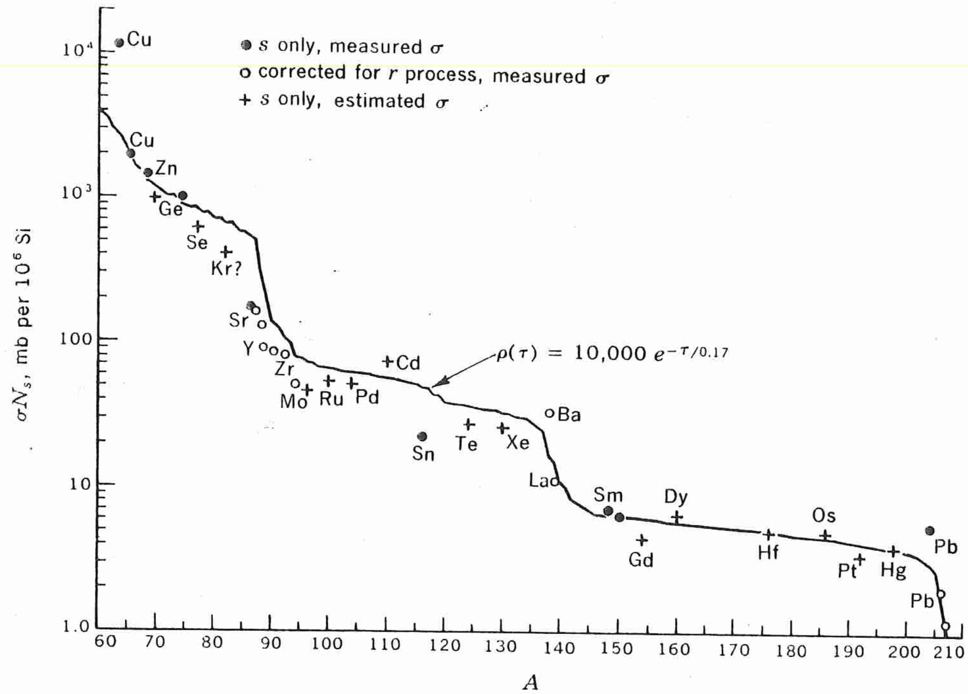

Fig. 7-20 The solar-system σN_s curve. The product of the neutron-capture cross sections for $kT = 30$ kev times the nuclide abundance per 10^6 silicon atoms is plotted versus the atomic mass number A. The solid curve is the calculated result of an exponential distribution of neutron exposures. [*P. A. Seeger, W. A. Fowler, and D. D. Clayton, Astrophys. J. Suppl.*, **11**:121 (1965). *By permission of The University of Chicago Press. Copyright 1965 by The University of Chicago.*]

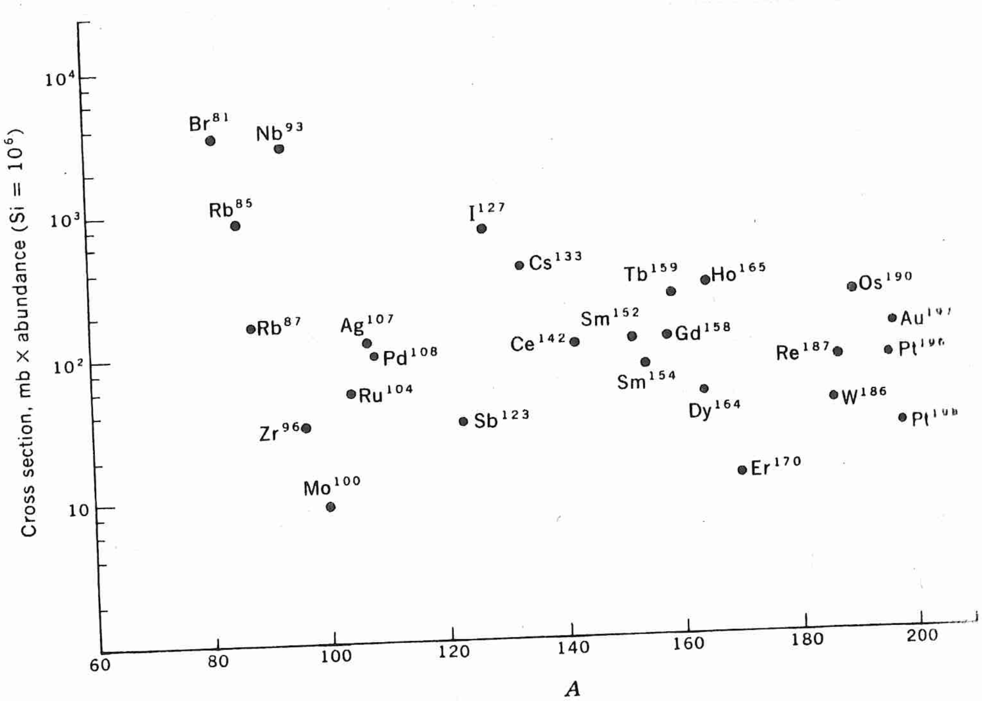

Fig. 7-21 The product of the neutron-capture cross section times the nuclide abundance for r-process nuclei. The irregularity in the product σN for these nuclei is expected and shows that the smooth variation found in Fig. 7-20 is not wholly accidental.

NEUTRON EXPOSURES

~~Notes~~·

NEUTRON FLUX $\phi(t)$

FLUENCE = EXPOSURE = IRRADIATION

$$\tau = \int \phi(t)\,dt = \int n(v)\,v\,dt$$

has dimensions of

$$\frac{1}{L^3} \cdot \frac{L}{T} \cdot T = L^{-2} \qquad [mb^{-1}]$$

IN ABSENCE OF BRANCHING,

$$\frac{dn_m(\tau)}{d\tau} = -\sigma_m(T)\,n_m(t) + \sigma_{m-1}(T)\,n_{m-1}(t)$$

IN STEADY FLOW

$$\frac{dn_m(\tau)}{dt} \simeq 0 \quad \text{or} \quad n\sigma \simeq \text{constant}$$

between magic N numbers

THEORY OF S-PROCESS

$m-1 \rightarrow m \rightarrow m+1$

- no branching
- all unstable nuclides decay before neutron capture

neutron density

$$\frac{dn_m(t)}{dt} = -\langle\sigma v\rangle_m n_m(t) N(t) + \langle\sigma v\rangle_{m-1} n_{m-1}(t) N(t)$$

Write $\langle\sigma v\rangle \equiv \sigma(T) V_T \hat{=}$ constant

$$\frac{dn_m(t)}{dt} = -V_T N(t) \left[\sigma_m(T) n_m(t) - n_{m-1}(t) \sigma_{m-1}(T)\right]$$

Define $d\tau = V_T N(t) dt$

$$\tau = \int V_T N(t) dt = \int \phi(t) dt$$

NEUTRON EXPOSURES – simplest case

^{56}Fe + increasing fluences

- small : build-up short of N=50
- bigger : N<50 fed thro' to ≤82
- bigger still N ≥82
- huge : pile up at Pb in
  Pb ⟷ Bi closed cycle.

– see Fig. 5 and especially Fig 7-27

SUCH YIELDS DO <u>NOT</u> RESEMBLE SOLAR S-ABUNDANCES

ARE SUCH YIELDS SEEN IN ANY r-PROCESS RICH STAR?

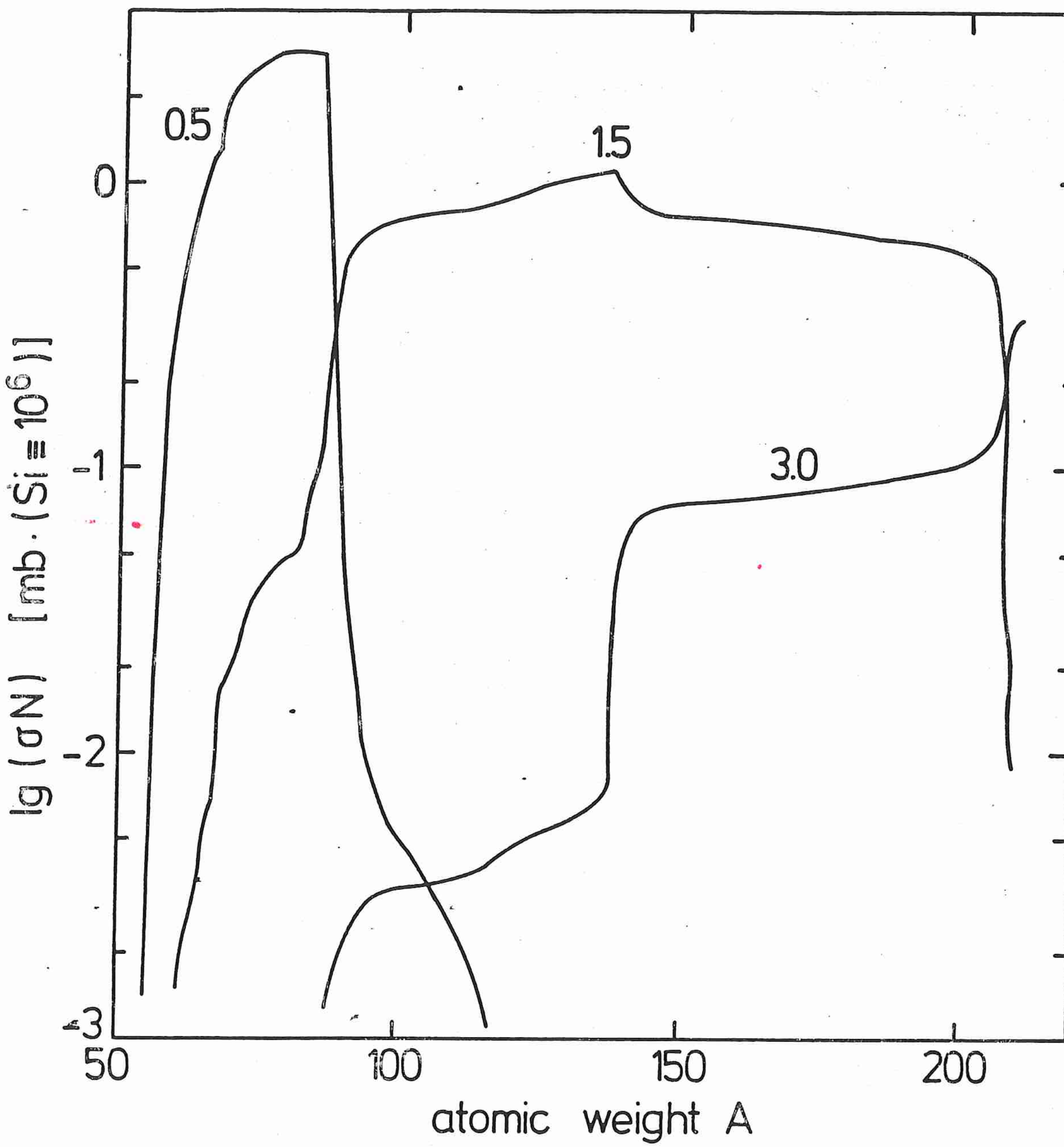

Fig. 5. Results of a model calculation solving eq.(3) for a seed of pure ^{56}Fe (at lg σN = 1.12). Different curves correspond to different values of the neutron exposure.

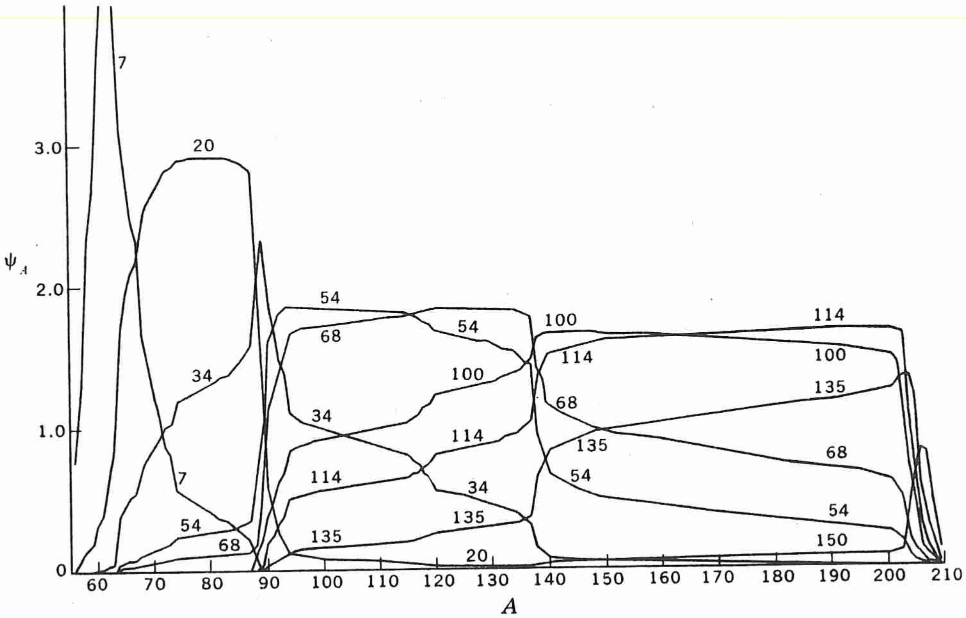

Fig. 7-22 The distributions $\psi_A = \sigma_A N_A$ for differing levels of neutron irradiation. Each curve is labeled by the parameter n_c, which is the average number of neutrons captured per initial iron seed nucleus. [*D. D. Clayton, W. A. Fowler, T. E. Hull, and B. A. Zimmerman, Ann. Phys.*, **12**:331 (1961).]

where $\rho(\tau)\,d\tau$ is the fraction of seed nuclei having received exposure τ in the interval $\tau \to \tau + d\tau$.

The exponential distribution of exposures was suggested to arise from the effect of galactic reprocessing, i.e. the total exposure experienced by some fraction of material would relate to the number of times that material had been processed through stars. With this choice of an exponential distribution of exposures, the set of differential equations (4.5) are amenable to a particularly simple analytic solution (Clayton and

A LITTLE HISTORY

B²FH 1957

σN vs A

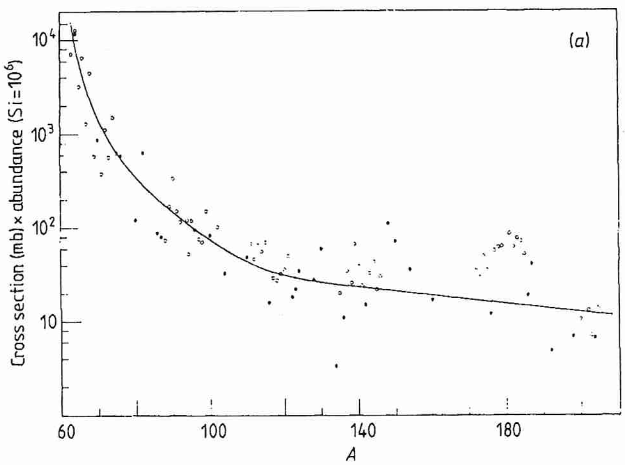

Clayton et al. (1961)

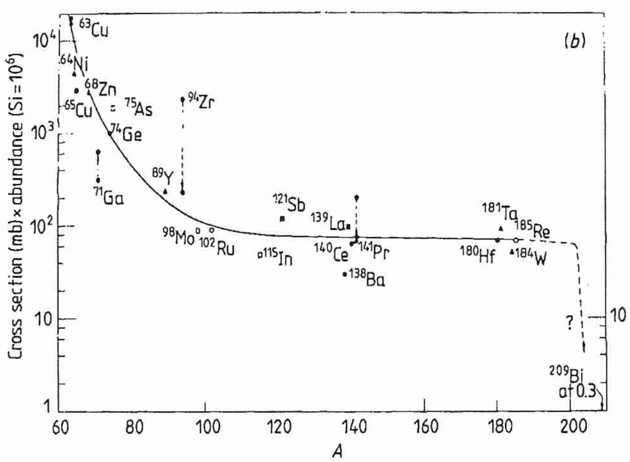

Figure 3. (a) The Solar-System s-process σN curve sketched in B²FH: ●, s process only; ○, s process predominantly. (b) The Solar-System s-process σN curve calculated in Clayton *et al* (1961). Oak Ridge: ●, s process, ○, s corrected for r-process contribution. Livermore: ▲, s process; △, s corrected. Average: ■, s process; □, s corrected. (c) The Solar-System s-process σN curve calculated in Seeger *et al* (1965). ●, s only, measured σ; ○, corrected for r process, measured σ; +, s only, estimated σ. (d) The Solar-System s-process σN curve calculated in Allen *et al* (1971). s only: ●, σ measured; ▲, σ estimated ○, σ measured. (e) The Solar-System s-process σN curve calculated in Käppeler *et al* (1982). ■, □, s-only isotopes; ○, predominantly s process. (f) The Solar-System s-process σN curve calculated in Ulrich (1973). ●, calculated, no branching; ◆, calculated, branching correction applied; ○, s only, measured σ; □, s(r), measured σ; △, s (r), measured σ; +, s only, estimated σ; ×, s, r, estimated σ. (g) The Solar-System s-process σN curve calculated in Beer *et al* (1984a, b). (h) The Solar-System s-process σN curve calculated in Mathews *et al* (1984a, b).

Seeger et al. 1965

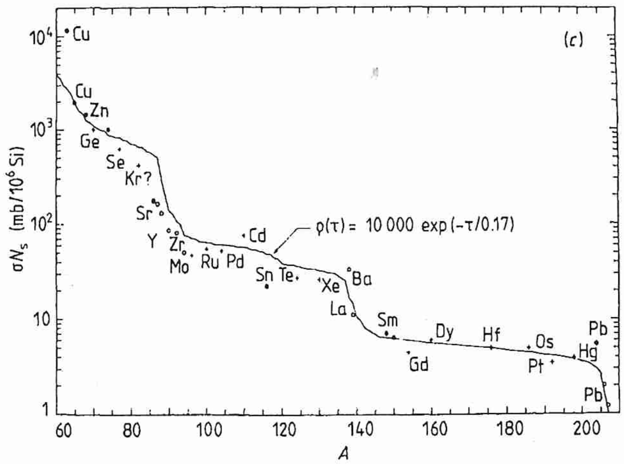

Allen et al. 1971

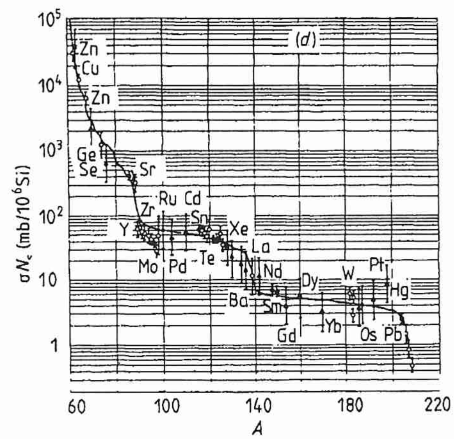

Kappeler et al. 1982

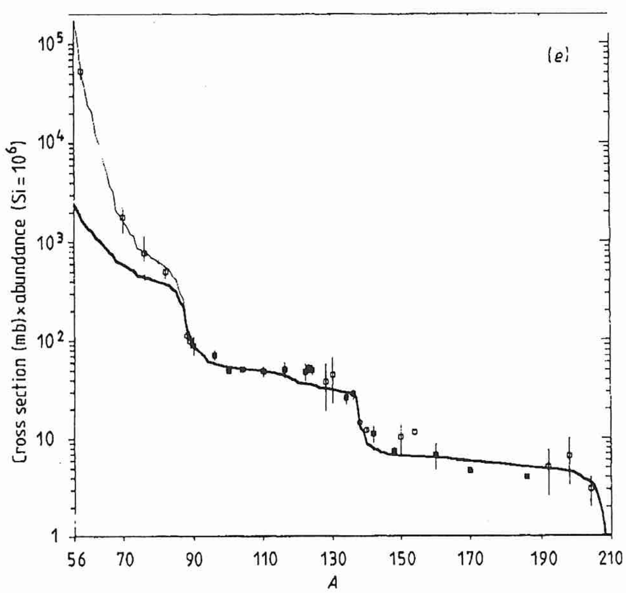

Figure 3 (*cont*).

Ulrich 1973

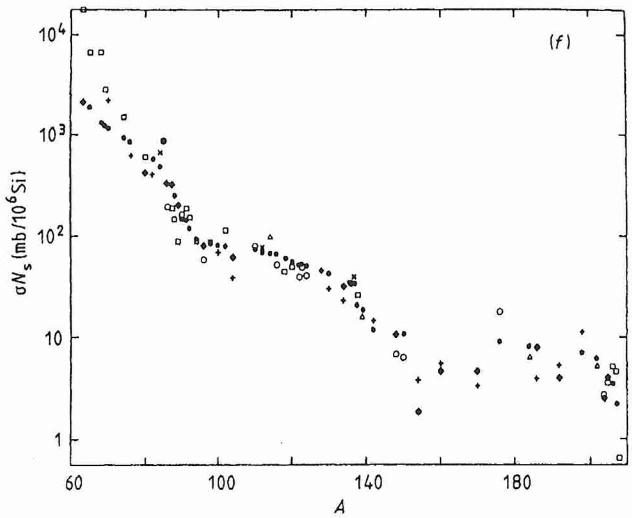

Beer et al. 1984

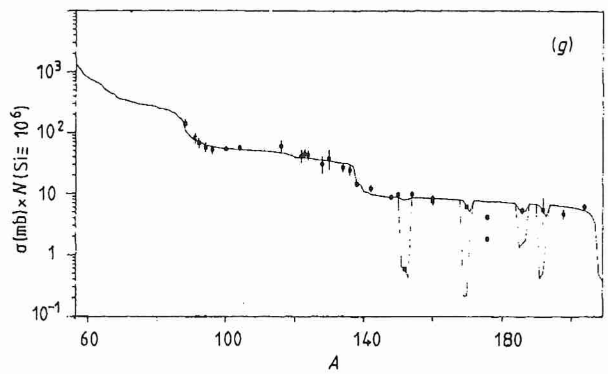

Mathews et al. 1984

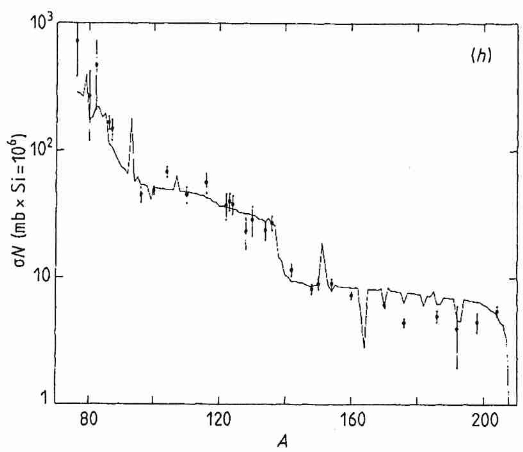

Figure 3 (*cont*).

WHAT IS $N(t)$ or $\tau(t)$
from SAD and/or from
candidate stellar sources?

- CLASSICAL APPROACH

PAGEL §6.2.2

- ASSUME ^{56}Fe = SEEDS

- EXPONENTIAL DIST'N OF EXPOSURES τ

$$\rho(\tau) = \frac{G N_{\odot}^{56}}{\tau_0} \exp(-\tau/\tau_0)$$

G = fraction of $N_{\odot}^{56}$ exposed to neutrons

τ_0 = mean (integrated) neutron exposure

ANALYTICAL SOLUTION TO SET OF dn_m/dt REQUIRE $N(t)$ & $\tau(k)$ be CONSTANT

$$\sigma_A N_S(A) = \frac{G N_{\odot}^{56}}{\tau_0} \prod_{i=56}^{A} \left(1 + \frac{1}{\sigma_i \tau_0}\right)^{-1}$$

and

$$\sigma_A N_S(A) = \frac{\sigma_{A-1} N_S(A-1)}{\left(1 + \frac{1}{\sigma_A \tau_0}\right)}$$

- CLASSICAL APPROACH modified for thermal pulse behavior
- EARLY variation for branches
  - WARD et al. (1976, ApJS, 31, 33)
- MORE ACCURATE $\sigma(n,\gamma)$ REVEALED INCONSISTENCIES, e.g.
  - ^{142}Nd ARLANDINI et al. 1999, ApJ, 525, 886

ADD ISSUES WITH CLASSICAL MODELS

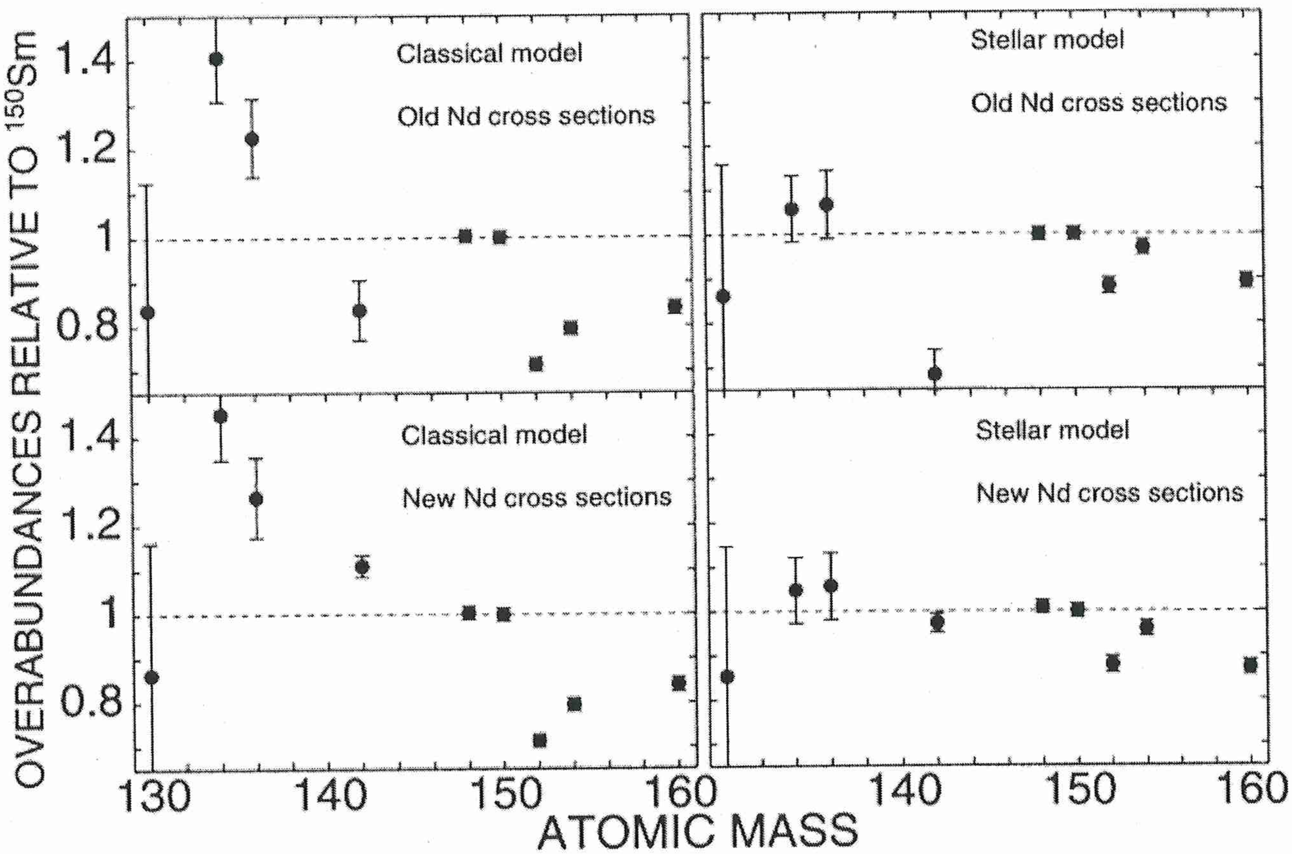
Classical model
Old Nd cross sections
Stellar model
Old Nd cross sections
Classical model
New Nd cross sections
Stellar model
New Nd cross sections
OVERABUNDANCES RELATIVE TO 150Sm
1.4
1.2
1
0.8
130
140
150
160
ATOMIC MASS

Arlandini et al. 1999, ApJ 525

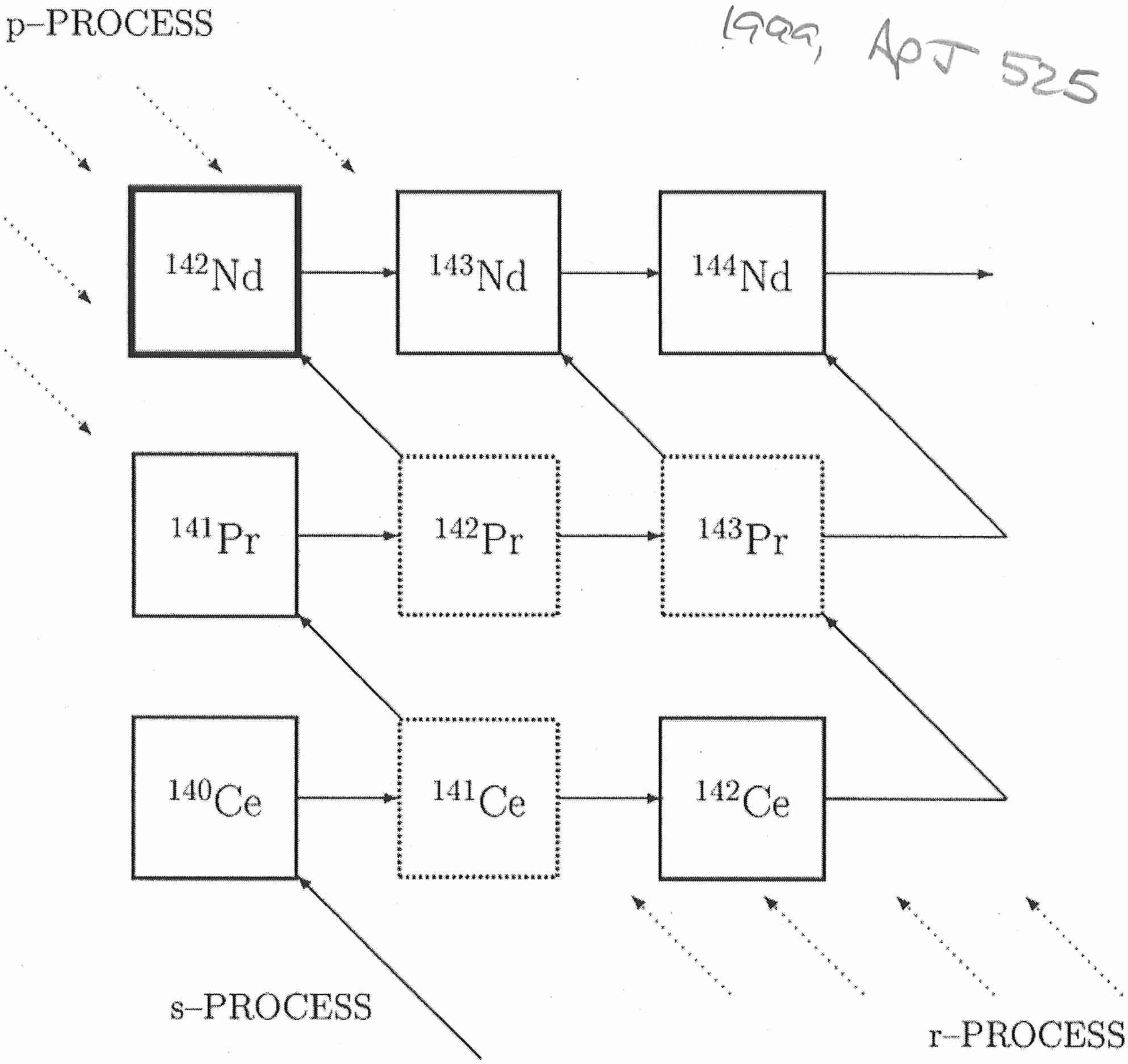

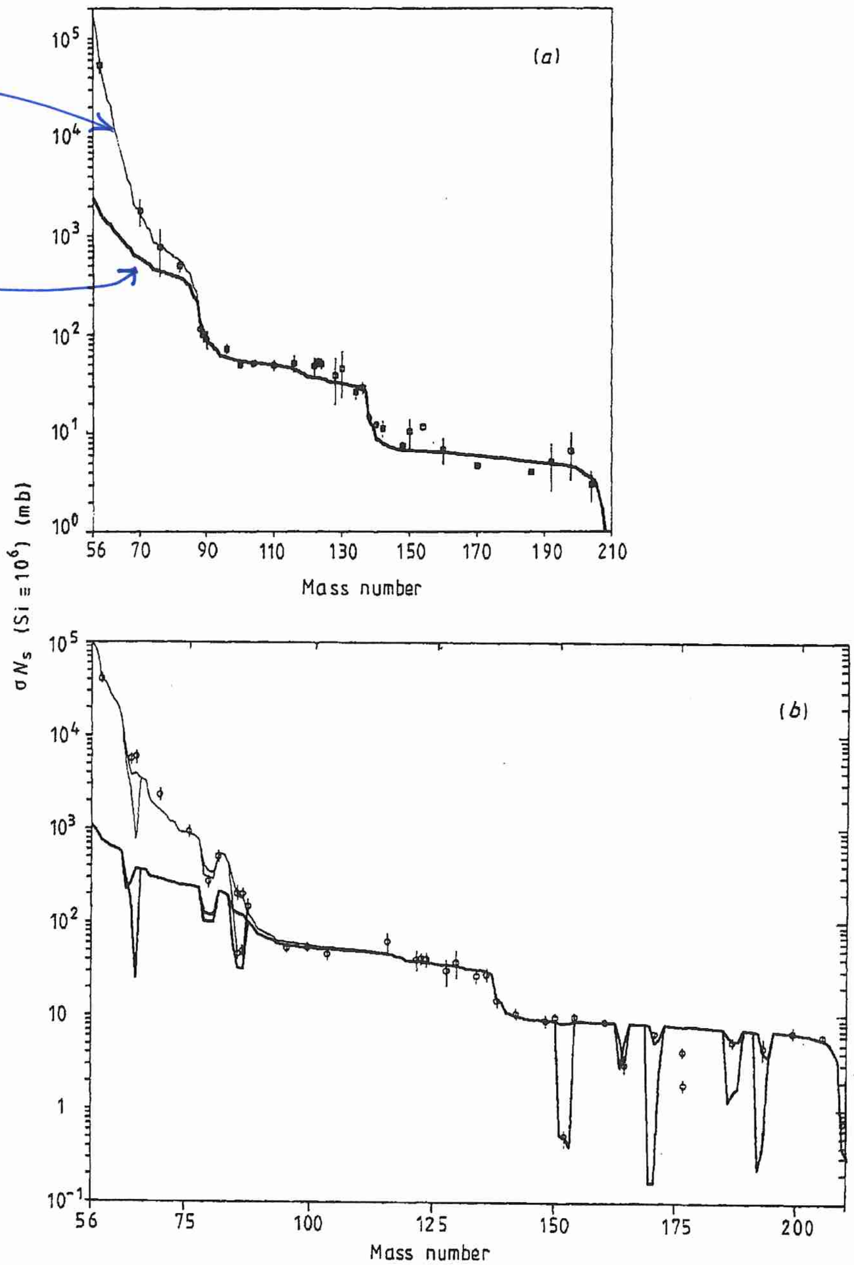

Figure 19. The characteristic product of cross section times s-process abundance versus mass number. We compare the status of this curve in 1982 (*a*) (with N_s from Cameron 1981) with the present situation (*b*) (N_s from Anders and Ebihara 1982). Symbols with error bars denote the empirical products of pure or almost pure s-isotopes.

25%, leading to good agreement of the ^{122,123,124}Te values with the model curve. Even more important was the revision of the rare-earth abundances. While the Gd abundance was lowered by 20%, most of the others were raised by ~10%. These changes yielded an empirical σN_s-value of Gd, which is now consistent with the model curve, and reduced also the step in the σN curve at the magic neutron number 82. As a result, the ratio between seed abundance and integral s-process yield for the main component

SAMPLE FIT

- KÄPPELER, BEER & WISHAK
  1989, Repts. Prog. in Physics 52, 945

- KÄPPELER et al.
  1990, ApJ, 354, 630

\+ . . . . . .

FITS DIFFER BECAUSE

- N(s) - only for SAD revised
- $\sigma(n,\gamma)$ - remeasured

LED TO

→ WEAK S-PROCESS
→ MAIN S-PROCESS
→ STRONG S-PROCESS

TERMINATION OF S-PROCESS

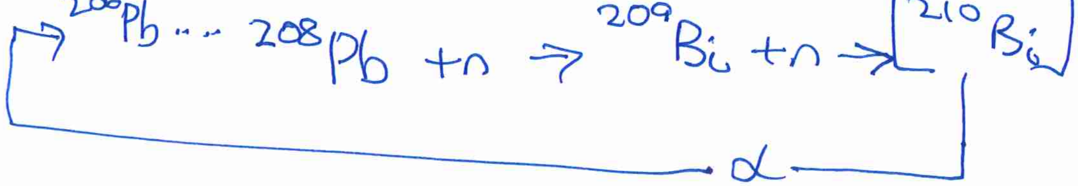

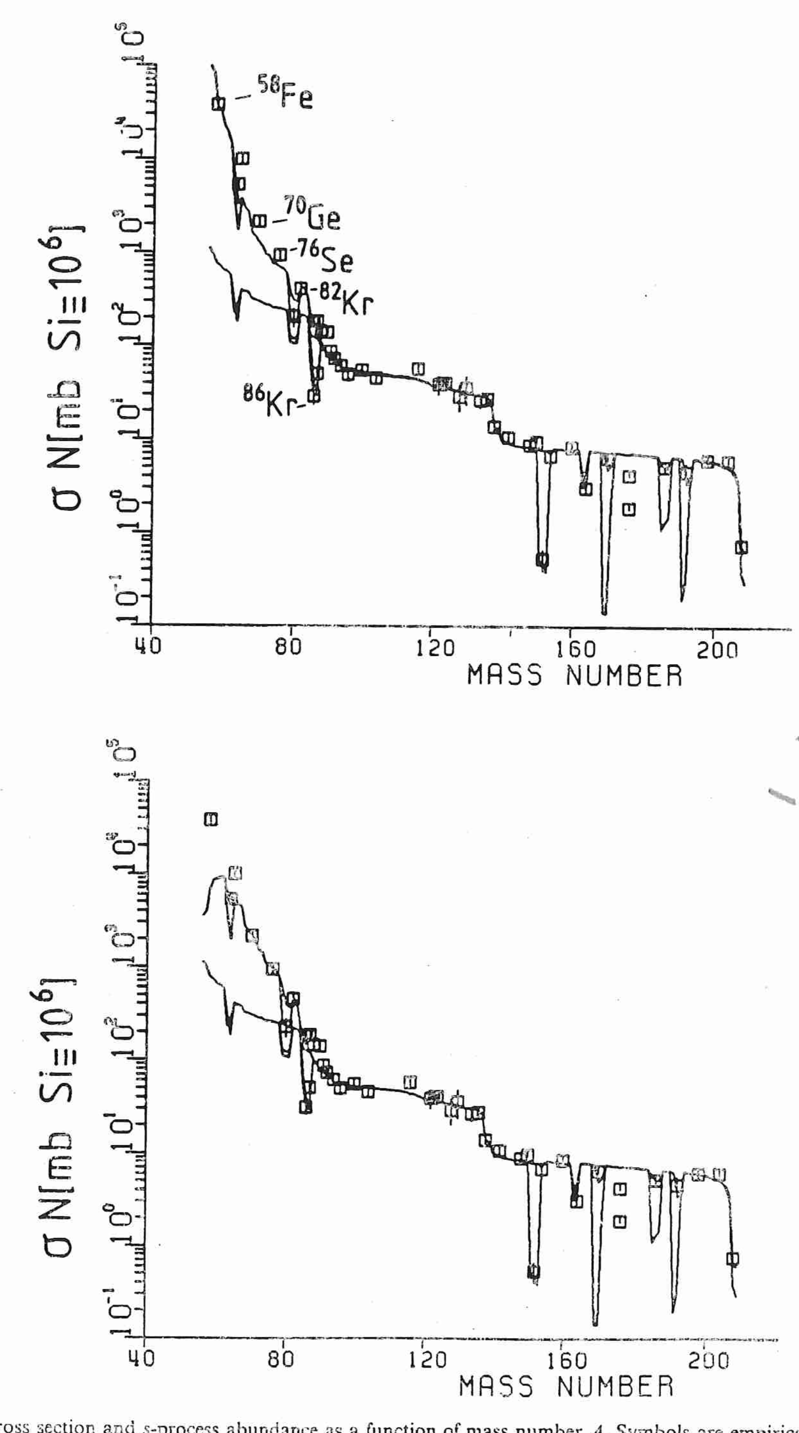

Fig. 4.—Product of capture cross section and *s*-process abundance as a function of mass number *A*. Symbols are empirical data. Significant branchings were [illegible] as a result of low empirical values on one of the branches. Below $A = 90$ the superposed weak component is effective. To reproduce the empirical data, an [illegible] with an exponential exposure distribution (*above*) and a single-flux *s*-process (*below*) are chosen. The second choice is clearly superior. The course of the [illegible] component in the region below $A = 90$ is also shown. Note that the ^{86}Kr and ^{87}Rb data located in the ^{85}Kr branching are not corrected for *r*-process [illegible]butions. Therefore, the theoretical calculations should remain below the empirical values to avoid overproduction.

weak s-proc.

difficult to distinguish – few nuclides – also p-process?

weak = single flux

but are extrapolated to $kT = 23$ keV according to the s-process temperature derived from branching analyses; in a few significant cases, the cross sections were also corrected for stellar enhancement factors. Branchings are considered only if they are strong enough to stand out on figure 19; the weaker branchings do not affect the abundances significantly, but can be important for estimating neutron density and temperature (see for example the branchings at $A = 147,148$ and at ^{134}Cs, ^{154}Eu, (§ 5.2.1). The branchings connected with the s-only isotopes ^{176}Lu, ^{176}Hf and ^{187}Os are complicated by long-lived radioactive decays. These decays are potential chronometers for the age of the s-process elements and will be discussed in some detail in § 7.

The weak and strong s-process components can alternatively be assumed to result from single neutron exposures. Such an assumption allows for a better reproduction of the s-only isotopes ^{70}Ge and ^{76}Se (Beer 1986, 1988, Beer and Macklin 1989); this is illustrated in table 4, where numerical σN_s-values for a single flux solution of the weak component are given in brackets in column 7. For possible stellar scenarios see § 6.

4.2. Neutron economy

The main difference between the σN_s curves in figure 19 comes from the revision of the rare-earth abundances by Anders and Ebihara (1982), giving rise to a much less pronounced step in the new σN_s curve at the magic neutron number 82. This corresponds to an increase of the mean neutron exposure, τ_0, and to a decrease of the required seed abundance, f. A comparison with the results for the 1982 curve (Käppeler *et al* 1982; Almeida and Käppeler 1983) is given in table 5.

Given the perfect agreement between the empirical σN_s-values and the calculated curve, one can be rather confident about the present s-process abundances. This statement is additionally supported by the smoothness of the related r-process abun-

BASIC DATA from CLASSICAL FITS

Table 5. Comparison of mean neutron exposure, τ_0, and fractional seed abundance, f, with values based on abundance compilations prior to Anders and Ebihara (1982). For a discussion of the neutron balance condition for the ^{22}Ne(α, n) source see the text.

	Käppeler *et al* (1982)	Present
Mean neutron exposure τ_0 (mb^{-1})		
Main component	0.24 ± 0.01	$(0.30 \pm 0.01)\left(\frac{kT(\mathrm{keV})}{30}\right)^{1/2}$
Weak component	0.056 ± 0.005	$(0.068 \pm 0.007)\left(\frac{kT(\mathrm{keV})}{30}\right)^{1/2}$
Strong component	—	7.0
Seed abundance, f (% of $N_\odot(^{56}\mathrm{Fe})$)		
Main component	0.092 ± 0.015	0.043 ± 0.002
Weak component	2.7 ± 0.2	1.6
Strong component	—	1.2×10^{-4}
Total number of neutrons captured per ^{56}Fe seed nucleus, Σn_c (equation (4.1))		
Main component	13.0[a]	15.1 ± 0.8
Weak component	—	2.8
Strong component	—	141.0

[a] Almeida and Käppeler (1983).

THESE ARE 'GCE-AVERAGED'

S-PROCESS BRANCHES

- EVEN AT $N(t) \to 0$, THERE IS NO SINGLE S-PROCESS PATH
- BRANCHES ARE INEVITABLE AND INSIGHTFUL
- SIMPLE CASE

  NUCLIDE WITH $\tau(\beta) \sim$ LONG

  AT $N(t) = 0 \to \beta$ DECAY

  $\gtrsim$ critical value $\to$ n-CAPTURE

S-PROCESS BRANCHES

POTENTIAL INFORMATION

- $N(n)$
- T_8
- τ
- t_8
- Age of s-process products
- $N(n_e)$

BUT INFORMATION OFTEN HELD BY ISOTOPIC ABUNDANCE RATIOS

- RATIOS FROM METEORITIC DATA
- FEWER RATIOS FROM STELLAR SPECTRA

A BRANCH OR TWO

- ^{85}Kr

N = 50 is MAGIC

$\therefore \sigma(^{87}Rb) \sim \frac{1}{10}\sigma(^{85}Rb)$

$\therefore$ ISOTOPIC ABUNDANCE of Rb DEPENDS ON PATH TAKEN and $\therefore$ on N(n)

MEASURE Rb|Sr|Y|Zr RATIOS

CANNOT GET $^{85}Rb/^{87}Rb$ (WHY?)

LTE for ^{85}Kr

WARD (1977

WARD + FOWLER (1980

85Kr.

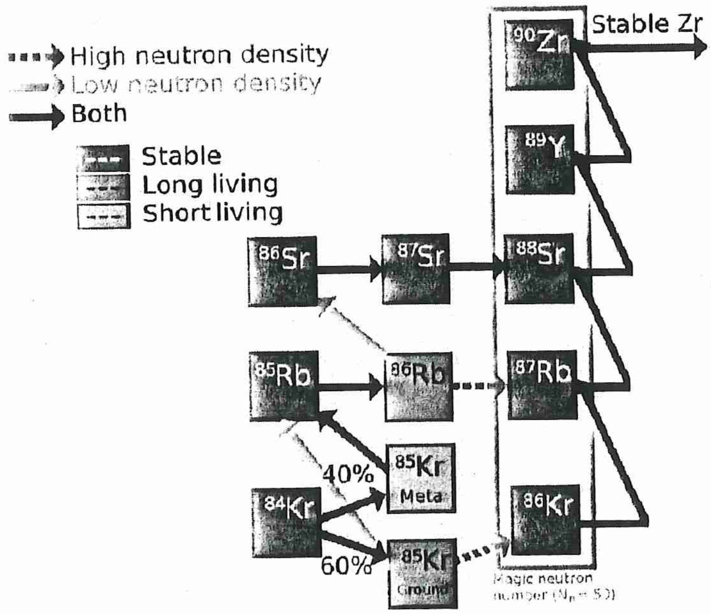

Fig. 32. Section of the chart of the nuclides from Kr to Zr. Stable isotopes are depicted with dark backgrounds and white labels. Unstable isotopes are depicted on a lighter background with black labels. The light arrow shows the neutron flow for low-neutron densities, whereas the dark, dashed arrows show the flow for high neutron densities ($N_n \geq 10^8$ n/cm^{-3}). The black solid arrows shows the direction of the flow for all densities. Isotope with magic neutron number = 50 are surrounded by the open rectangle. Figure provided by Mark van Raai

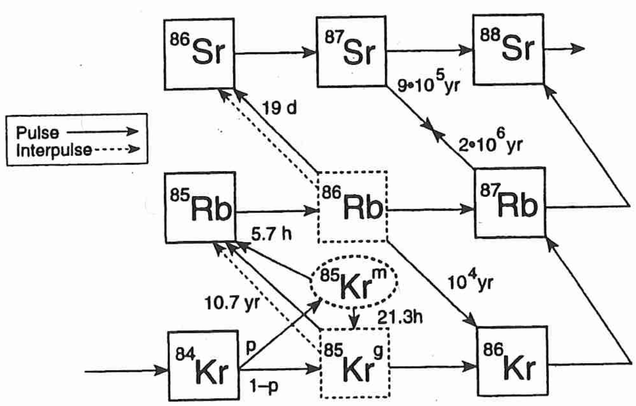

FIG. 8.—Synthesis of Kr, Rb, and Sr isotopes during a thermal pulse (*solid line*) and in the interpulse phase (*dashed lines*) when the ^{85}Kr and ^{86}Rb which are built up decay. The population p of the isomeric state of ^{85}Kr is generated by neutron capture on ^{84}Kr ($p = 0.52 \pm 0.006$; Beer et al. 1991). Half lives of unstable nuclei are indicated and, when temperature dependent, a temperature of 30 keV has been adopted. The time scales for ^{87}Rb and ^{87}Sr β-decay during the pulse are too long to be of any significance for the synthesis. The branching of ^{86}Rb to ^{96}Kr can be neglected too. The unstable nuclei ^{85}Kr and ^{86}Rb are represented by "broken" boxes; ^{87}Rb is effectively stable after manufacture. (After Beer & Macklin 1989.)

LAMBERT et al.

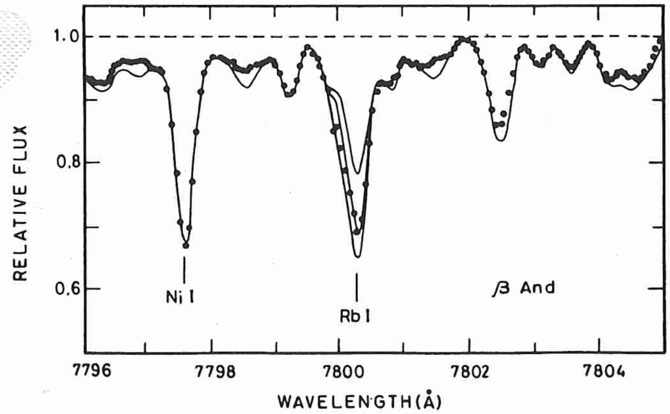

FIG. 2.—Observed (*filled circles*) and synthetic spectra (*thin lines*) of the M giant β And around the Rb I 7800 Å line. Synthetic spectra are shown for the Rb abundances [Rb/M] = −0.7, −0.4, and −0.1.

overabundances of Nd and other rare-earths but moderate overabundances of the lighter *s*-process elements such as Sr, Y, and Zr. Unidentified lines presumably attributable to rare earth atoms or ions are quite numerous around 7800 Å (and elsewhere) and two are labeled in Figure 5.

Our results are summarized in Table 1, where the stellar parameters (T_{eff}, g), metallicity [M/H], and the *s*-process enhancement [*s*/M] are taken from Smith & Lambert (1990), where *s* here denotes Y and Zr. The fit of the synthetic spectra to the observed spectrum gives [Rb/M] which is computed from [Rb/H] and [M/H]. This [M/H] is not necessarily identical to the value given by Smith & Lambert (1990), but, as explained above, [Rb/M] is insensitive to how the TiO lines and quasi-continuous opacity are represented. In expressing the stellar Rb abundances as [Rb/M] on [Rb/H], we adopt the meteoritic Rb abundance given by Anders & Grevesse (1989): log ϵ(Rb) = 2.4 ± 0.03. The solar photospheric Rb abundance based on published (Hauge 1972) and unpublished (Grevesse 1984) analyses of the 7800 and 7947 Å Rb I lines is slightly higher: log ϵ(Rb = 2.60 with ±0.15 as an estimated uncertainty. If the photospheric Rb abundance is preferred as the reference point, the [Rb/M]-values in Table 1 will have to be

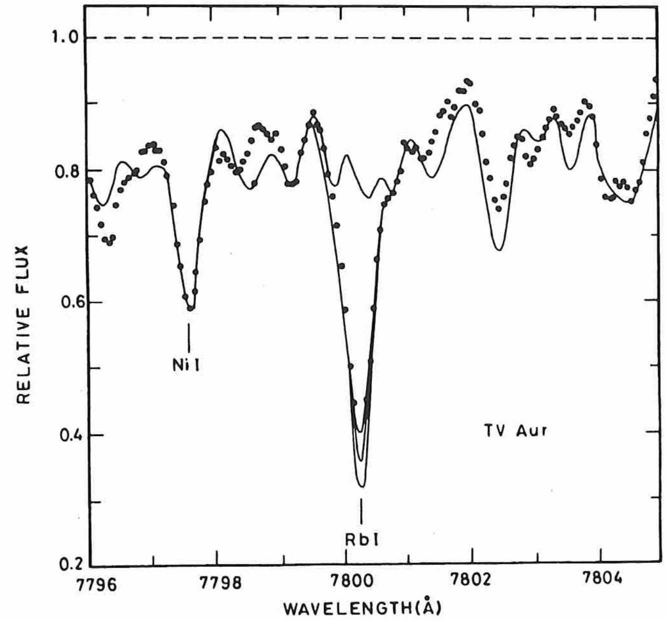

FIG. 4.—Observed (*filled circles*) and synthetic spectra (*thin lines*) of the cool intrinsic S star TV Aur around the Rb I 7800 Å line. Synthetic spectra are shown for [Rb/M] = +1.2, 0.9, 0.6, and −5 (no Rb).

decreased by 0.2. The presence or absence of Tc is noted in Table 1: intrinsic MS/S stars have Tc and the extrinsic (binary) MS/S stars do not have Tc.

3.3. *The s-process Rubidium in MS/S and Barium Stars*

In material of solar system composition, the *s*-process in the Kr-Rb region is resolvable into two components having different origins in terms of physical parameters and presumably of stellar sites (see Käppeler et al. 1989). The "weak" component, which is the dominant contributor to elements lighter than about Kr, is probably synthesized in the He-burning layers of massive stars. The "main" component, which is the dominant contributor to elements heavier than about Kr, is synthesized in the He shell of low-mass AGB stars and is the component whose effects are seen in the MS/S and barium stars. In addi-

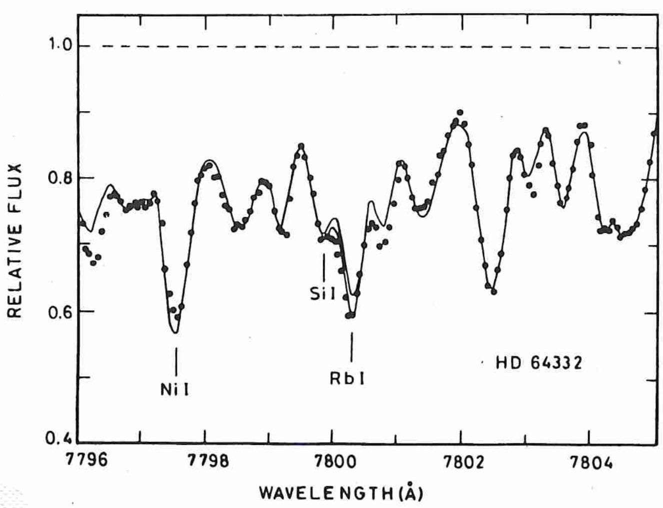

FIG. 3.—Observed (*filled circles*) and synthetic spectra (*thin lines*) of the intrinsic S star HD 64332 around the Rb I 7800 Å line. Synthetic spectra are shown for [Rb/M] = +0.2 and 0.0.

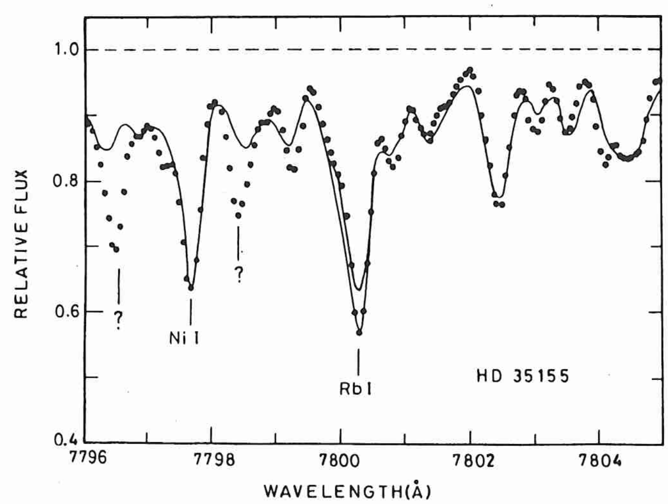

FIG. 5.—Observed (*filled circles*) and synthetic spectra (*thin lines*) of the extrinsic S star HD 35155 around the Rb I 7800 Å line. Synthetic spectra are shown for [Rb/M] = +0.1 and −0.2.

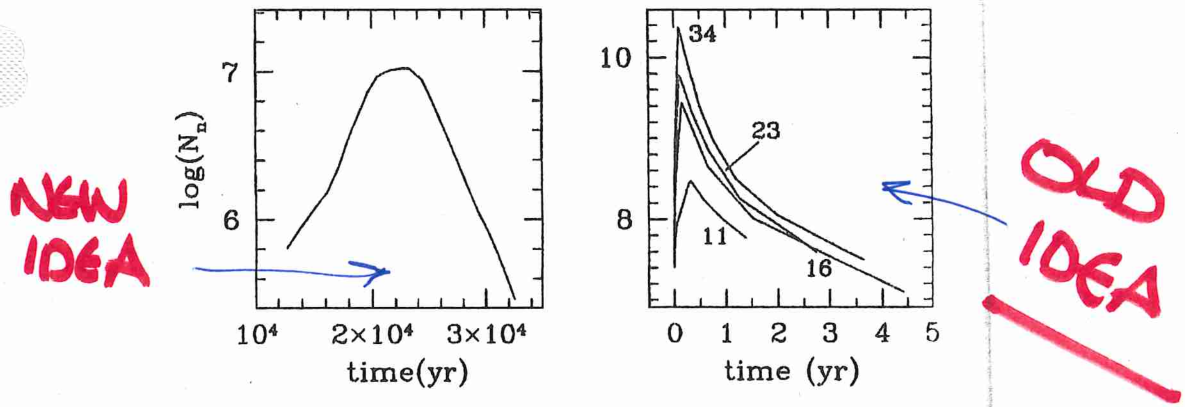

Figure 11 Neutron density during slow neutron capture processing in thermal-pulsing asymptotic giant branch stars. *a*. The situation in the central layer of the radiative zone where ^{13}C burns in the interpulse period, according to the schematic model of Gallino et al (1998). *b*. Neutron density from activation of the ^{22}Ne(α,n)^{25}Mg neutron source in different pulses. The bottom temperature increases with pulse number (11, 16, etc.) as does the neutron density.

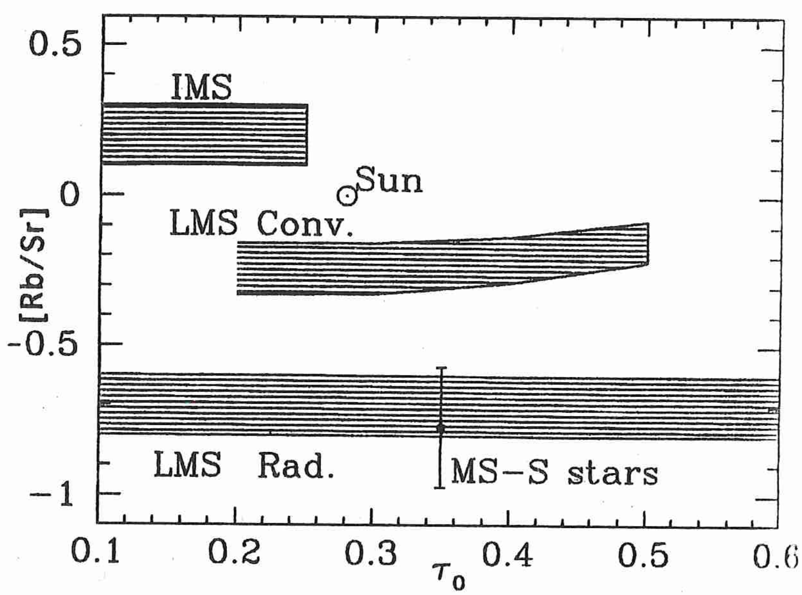

Figure 14 The average abundance ratio Rb/Sr, as deduced by Lambert et al (1995) from measurements in MS and S stars. The shaded regions cover the predictions we derive from *s*-process models in IMS and in LMS. In the first case, neutrons are produced by ^{22}Ne burning and in the second by ^{13}C burning. Convective (*Conv.*) and radiative (*Rad.*) ^{13}C burnings are shown, and it is clear that the convective model prediction is far above the observed value, whereas the radiative model is consistent with the data on MS stars.

Abia et al. (2001)

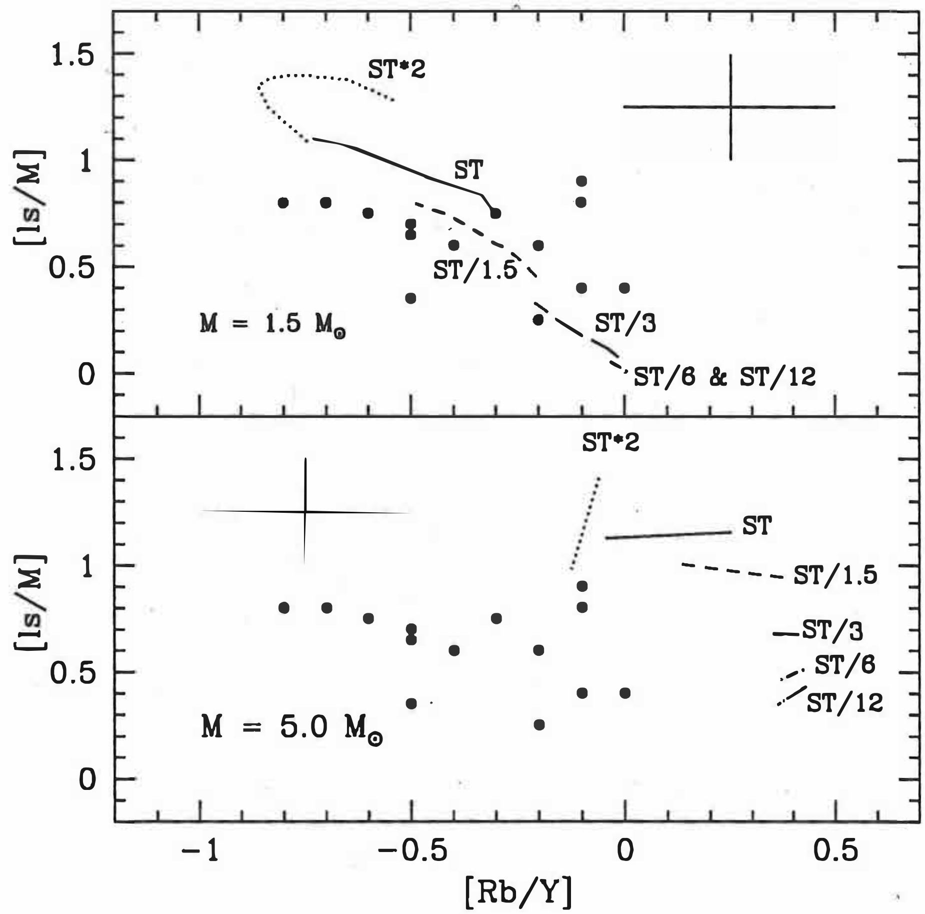

FIG. 5.—Comparison of the observed mean low-mass *s*-element (Y, Zr) enhancement (signature of the neutron exposure) against [Rb/Y] (signature of the neutron density) with theoretical predictions for a 1.5 $M_{\odot}$ (*top*) and 5 $M_{\odot}$ (*bottom*) TP-AGB star for different parameterizations of the ^{13}C pocket (*lines*). The theoretical predictions shown are for stellar models with C/O ~ 1 and metallicity [Fe/H] $\gtrsim -0.3$, which is the metallicity of most of the stars studied here. Only stars in the sample with metallicity above this value are plotted (see text). Note that several stars coincide in the same data point.

^{85}Kr BRANCH

- MS-S STARS

  LAMBERT et al. 1995

  → $^{13}C(\alpha, n)^{16}O$ in RADIATIVE INTERPULSE INTERVAL

- CARBON STARS

  ABIA et al. 2001 ApJ 559, 1117

  * NO SPECTRA ILLUSTRATED!